Atomic Force Microscopy

Alexandre Dazzi, Institut de Chimie Physique
alexandre.dazzi@universite-paris-saclay.fr

80’s, strong willing to manipulate and observe nanometric objects

Optical Microscopy

res ≈ 300 nm

$$res = \frac{\lambda}{2NA}$$

Electron Microscopy

res ≈ 0.1 nm

« Feeling is better than seeing »
or the born of nanotechnology

Gerd Binnig

(Physics Nobel Prize 1986)

1985 Atomic Force Microscope

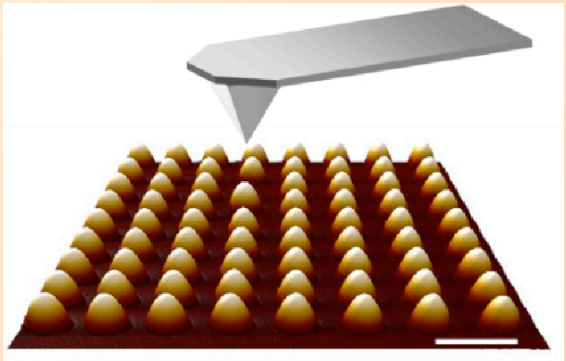

- Silicon tip to palpate the surface.
- Cantilever to move the tip.
- No constraint on the surface nature

II. Tip-surface interaction

How to describe the tip-surface

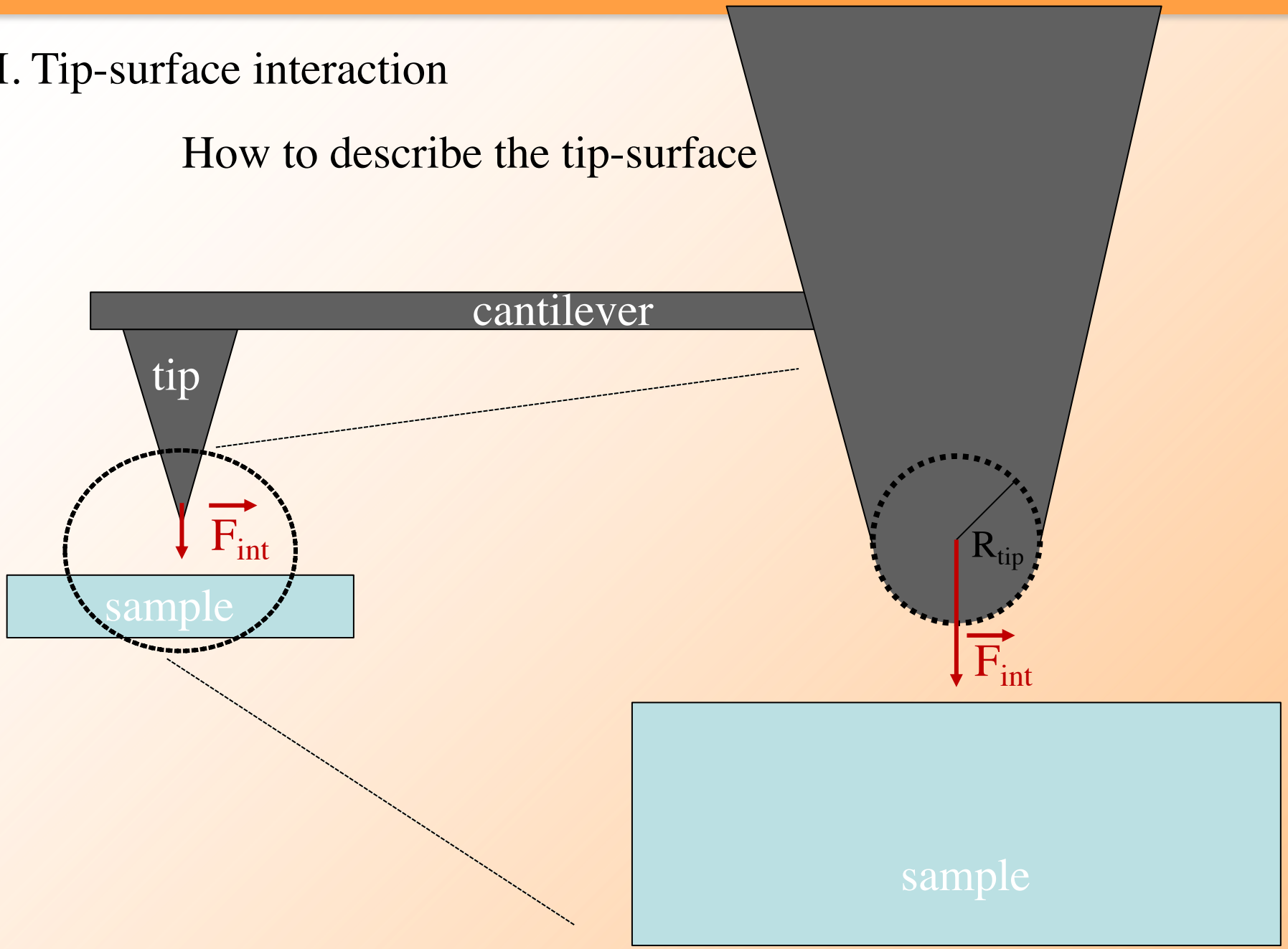

A) Atom-atom interaction

Lennard-Jones potential describes the interaction between atoms or small molecules.

$$V(r) = \frac{A}{r^{12}} - \frac{B}{r^{6}}$$

A,B constant related to nature of atoms and r distance between atoms

Repulsive interactions

Attractive interactions
(Van der Waals)

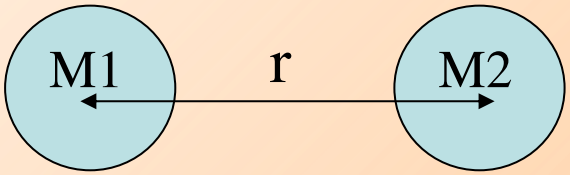

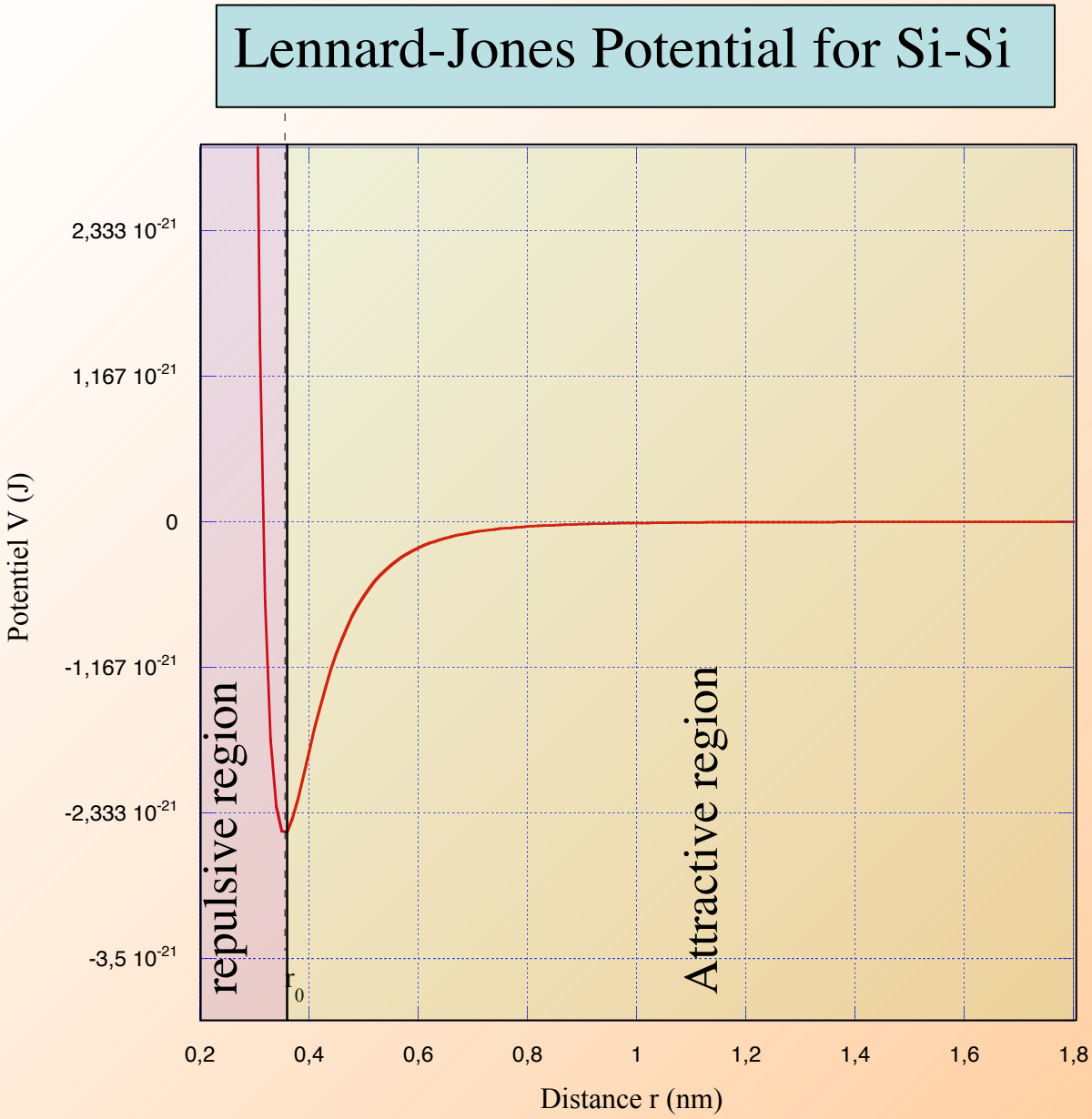
Lennard-Jones Potential for Si-Si
2,333 10-21
1,167 10-21
0
-1,167 10-21
-2,333 10-21
-3,5 10-21
Potentiel V (J)
repulsive region
Attractive region
r0
0,2
0,4
0,6
0,8
1
1,2
1,4
1,6
1,8
Distance r (nm)

B) Tip-surface interaction

B.1) Attractives forces

$$\vec{F}_{att} = \frac{6B}{r^7}$$

(Van der Waals)

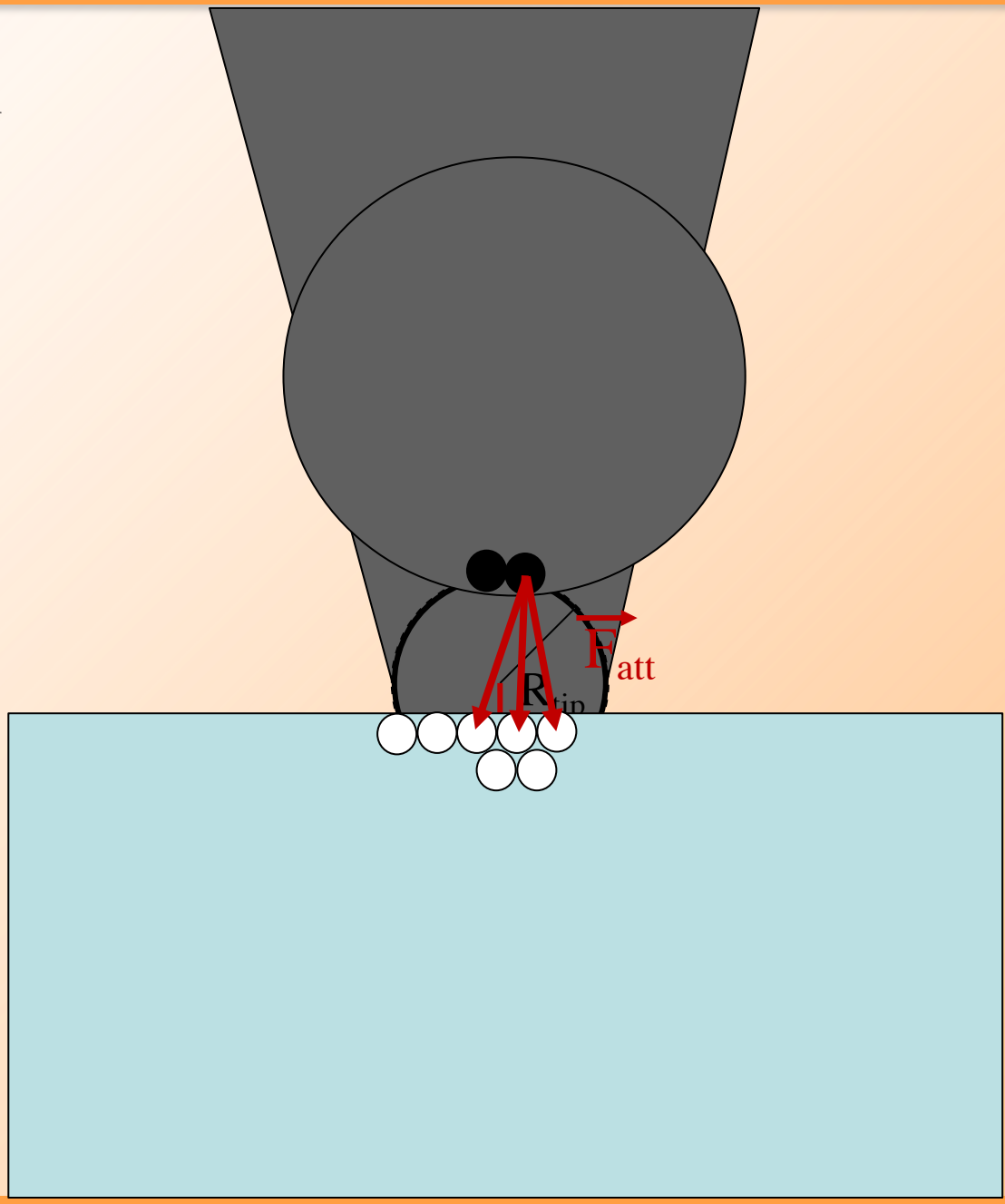

B.1) Attractives forces for a sphere-plane interaction

$$\overrightarrow{F_{att}^{s-p}} = -\frac{HR}{6D^2}$$

H Hamaker constant, R radius of the tip,
D distance bertween tip and sample surface

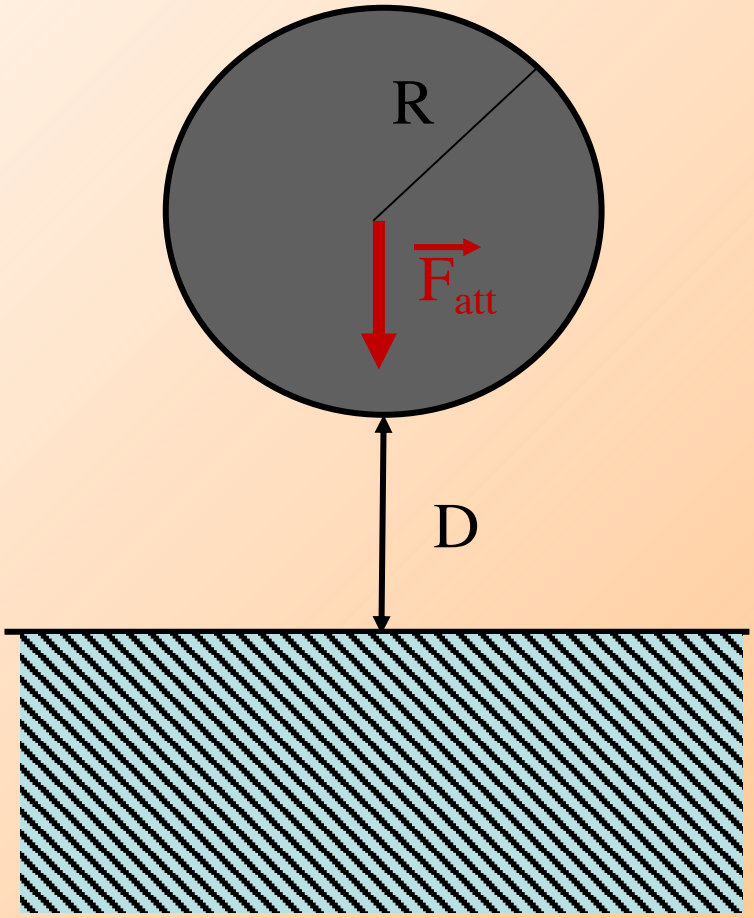

B.2) Repulsive forces for a sphere-plane interaction

B.2.1) Hertz contact

$$F_{rep} = \frac{4}{3} E^* \sqrt{R} h^{3/2}$$

h indentation
a radius of contact area
R radius of the sphere
E Young modulus
ν Poisson coefficient

$$\frac{1}{E^*} = \frac{1-{\nu_1}^2}{E_1} + \frac{1-{\nu_2}^2}{E_2}$$

$$\frac{1}{R} = \frac{1}{R_1} + \frac{1}{R_2} \qquad h = \frac{a^2}{R}$$

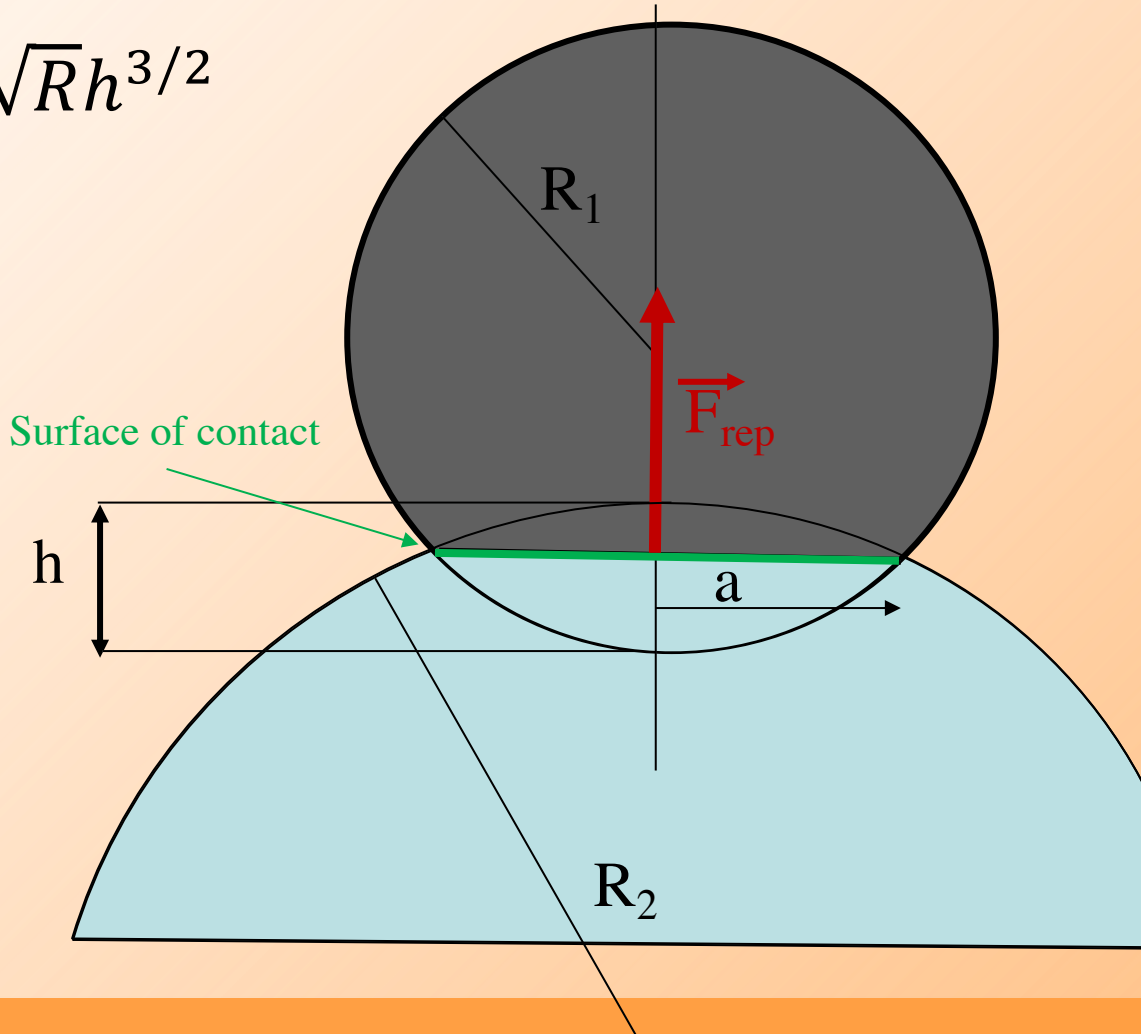

B.2) Repulsive forces for a sphere-plane interaction

B.2.2) Sphere-plane

$$F_{rep} = \frac{4}{3} E^* \sqrt{R_{tip}} h^{3/2}$$

$$\frac{1}{E^*} = \frac{1 - \nu_{tip}{}^2}{E_{tip}} + \frac{1 - \nu_{sample}{}^2}{E_{sample}}$$

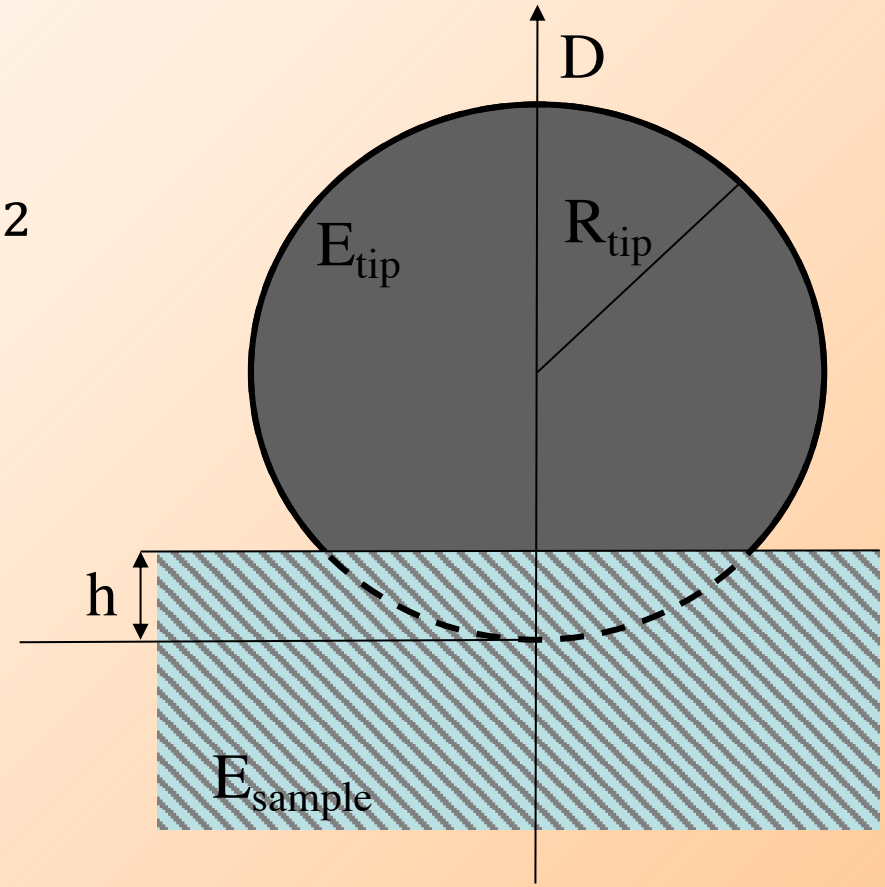

B.2) Repulsive forces for a sphere-plane interaction

B.2.2) Sphere-plane

How to define the distance of contact ?

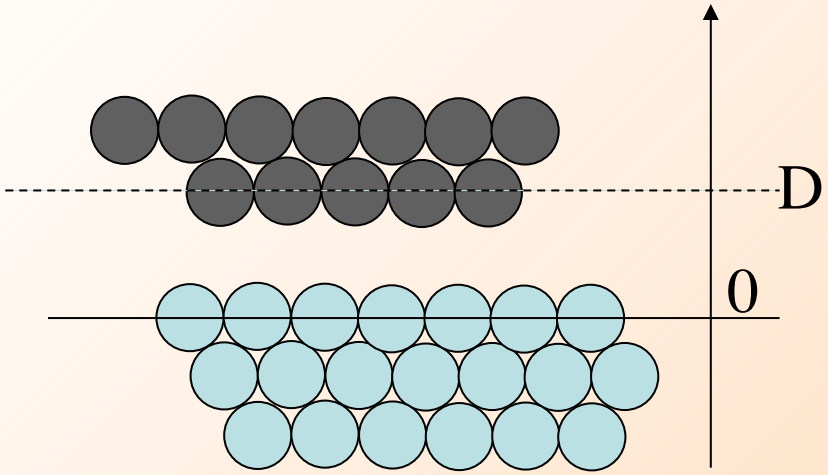

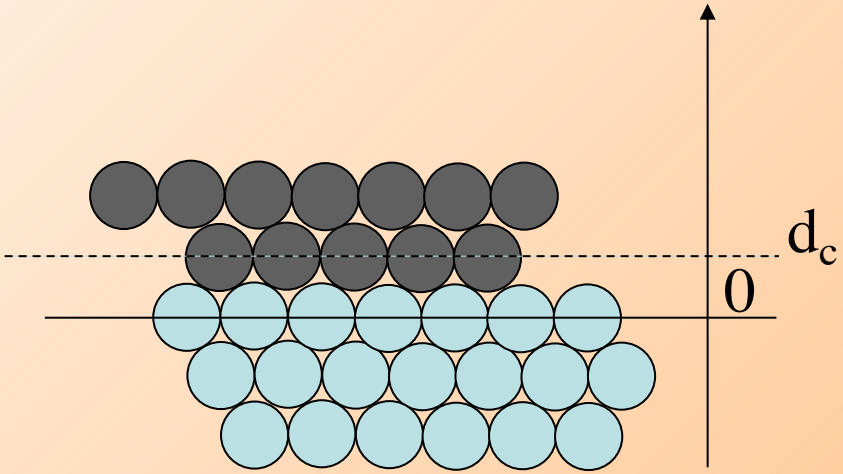

d_c=0.165 nm

B.2) Repulsive forces for a sphere-plane interaction

B.2.2) Sphere-plane

$$F_{rep} = \frac{4}{3} E^* \sqrt{R_{tip}} (d_c - D)^{3/2}$$

Where $D<d_c$
(only true in contact)

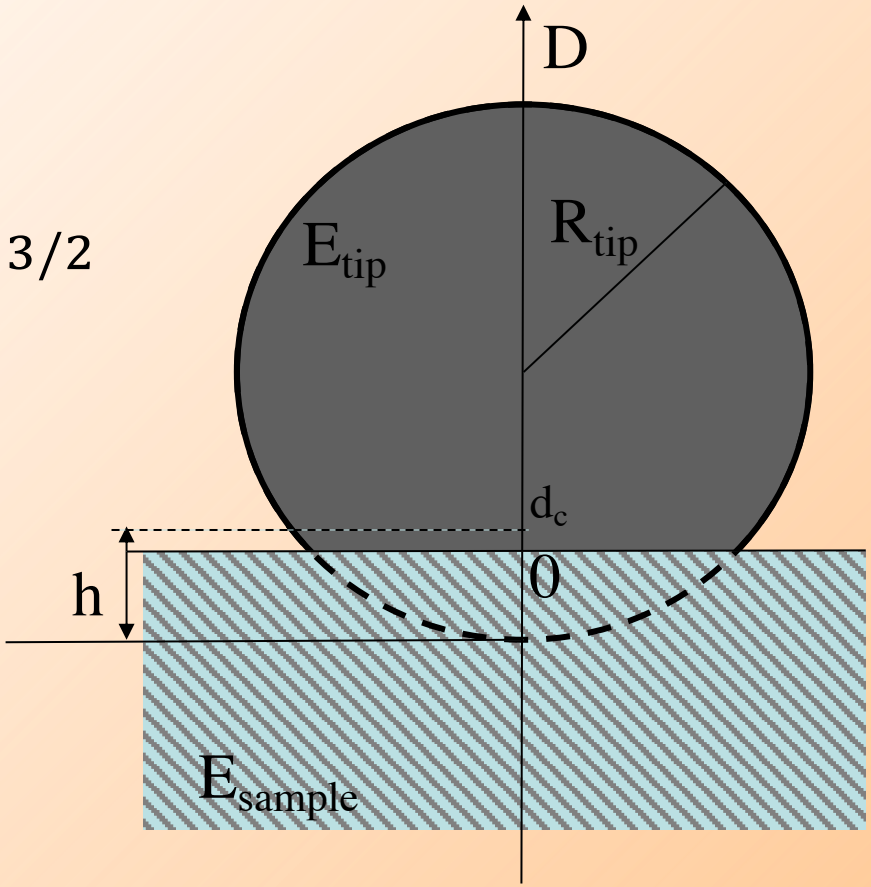

In D=dc, $\overrightarrow{F_{rep}} = 0$

but $\overrightarrow{F_{att}^{s-p}} = -\frac{HR_{tip}}{6{d_c}^2}$

B.3) Sphere-plane interaction force

$$\overrightarrow{F^{s-p}} = \begin{cases} -\dfrac{HR}{6D^2}\ \overrightarrow{u_z} & \text{If } D > d_c \\ \dfrac{4}{3}E^*\sqrt{R_{tip}}(d_c - D)^{3/2} - \dfrac{HR_{tip}}{6{d_c}^2}\ \overrightarrow{u_z} & \text{If } D \le d_c \end{cases}$$

$$\frac{1}{E^*} = \frac{1-{\nu_{tip}}^2}{E_{tip}} + \frac{1-{\nu_{sample}}^2}{E_{sample}}$$

DMT model (Derjagin-Muller-Toporov)

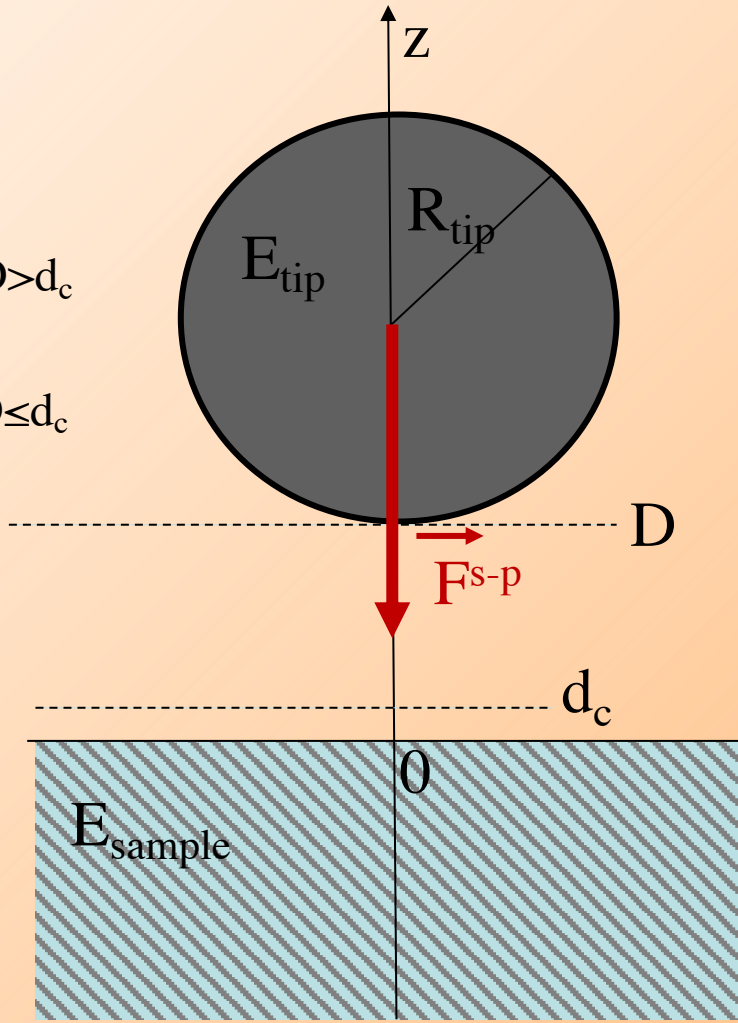

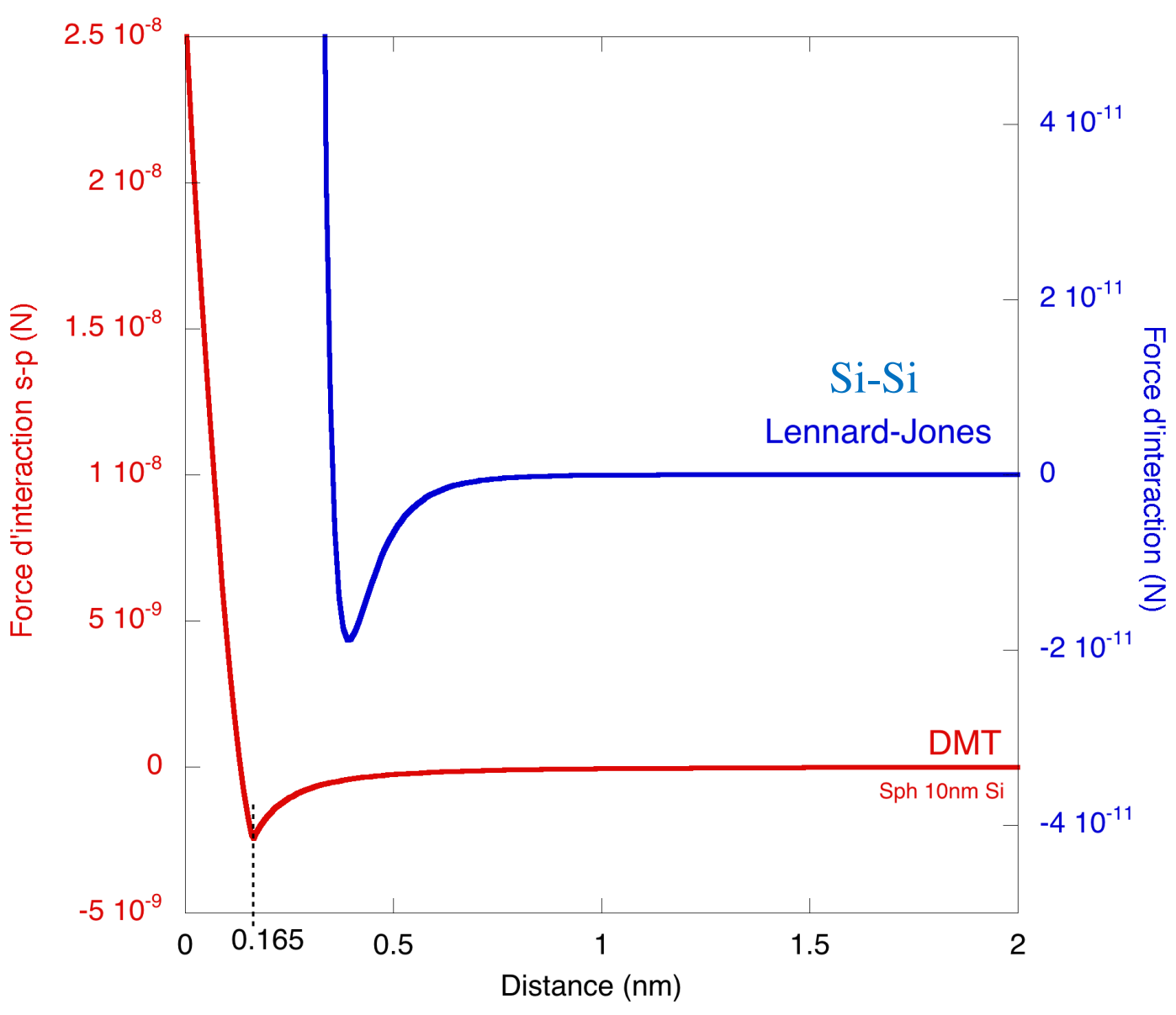
2.5 10-8
2 10-8
1.5 10-8
1 10-8
5 10-9
0
-5 10-9
Force d'interaction s-p (N)
4 10-11
2 10-11
0
-2 10-11
-4 10-11
Force d'interaction (N)
Si-Si
Lennard-Jones
DMT
Sph 10nm Si
0
0.165
0.5
1
1.5
2
Distance (nm)

III. Interaction force detection

A) Use of a cantilever to feel the force

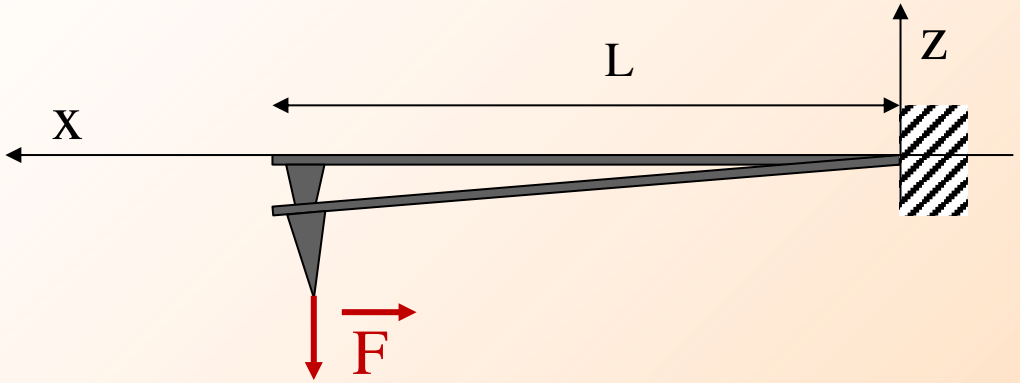

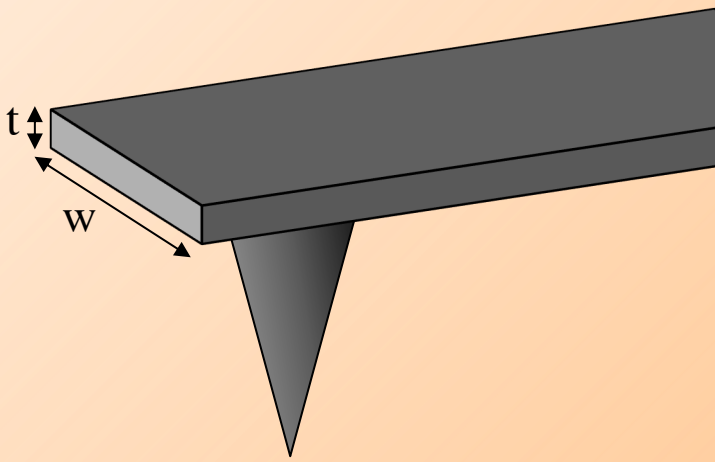

Bending moment : $M_f = -F(x - L)$

Euler-Bernouilli equation : $M_f = \mathrm{EI}\dfrac{\partial^2 z}{\partial x^2}$

E, Young's modulus of the cantilever

I, area moment of inertia of the cantilever cross section $I = \dfrac{wt^3}{12}$

Euler-Bernouilli equation :

$$-F(x-L) = \mathrm{EI}\frac{\partial^2 z}{\partial x^2}$$

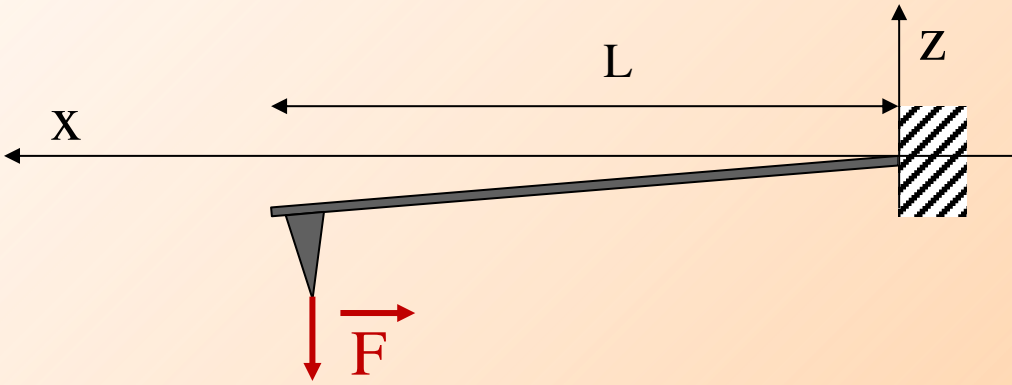

$$\frac{\partial^2 z}{\partial x^2} = \frac{F}{EI}(L-x)$$

Boundaries conditions :

$$\begin{cases} z(0) = 0 \\ \left.\dfrac{\partial z}{\partial x}\right|_{x=0} = 0 \end{cases}$$

$$z(x) = \frac{F}{EI}\left(\frac{1}{2}Lx^2 - \frac{1}{6}x^3\right)$$

B) Deflection measurement

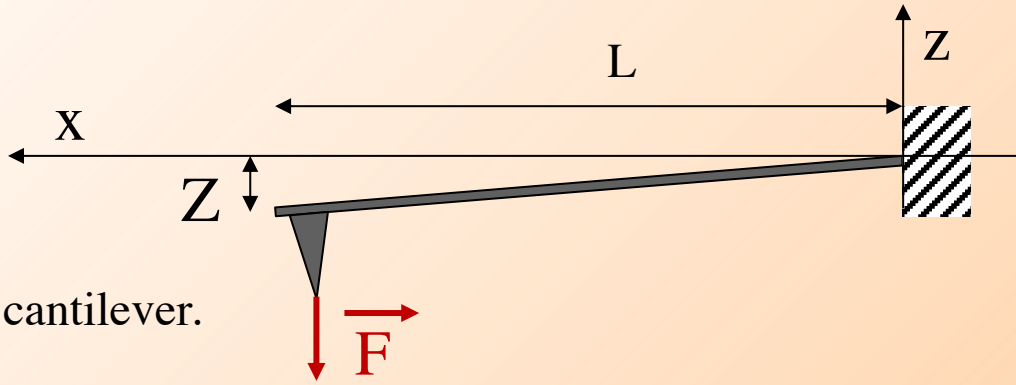

Deflection Z, is the flexure at the end of the cantilever.

$$Z = z(L) = \frac{F}{EI}\left(\frac{1}{2}LL^2 - \frac{1}{6}L^3\right) = \frac{FL^3}{3EI}$$

$$F = k_c Z \qquad \text{(Hooke's law)}$$

with k_c the stiffness of the cantilever

$$k_c = \frac{3EI}{L^3}$$

Si Cantilever

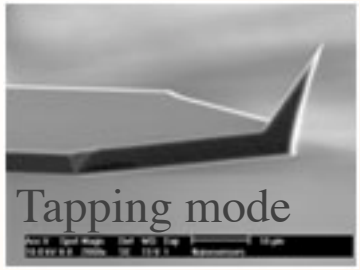

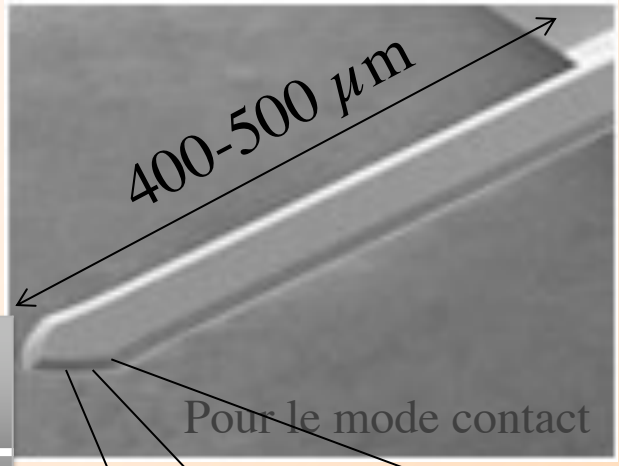

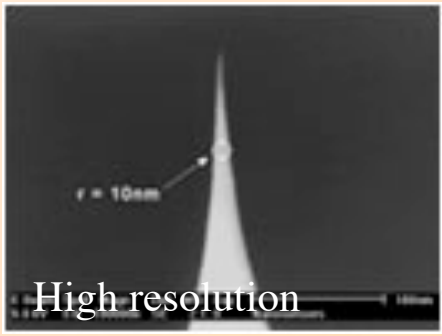

contact	**L=450 μm**	**k=0.1 N/m**	**f = 6 kHz**
tapping	**L=225 μm**	**k=40 N/m**	**f= 150 kHz**

Apex curvature radius 10 nm

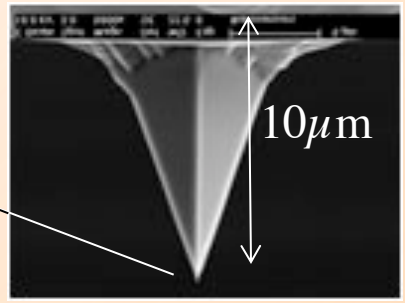

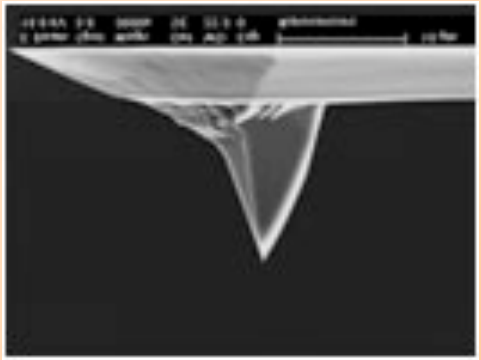

Optical detection of the force

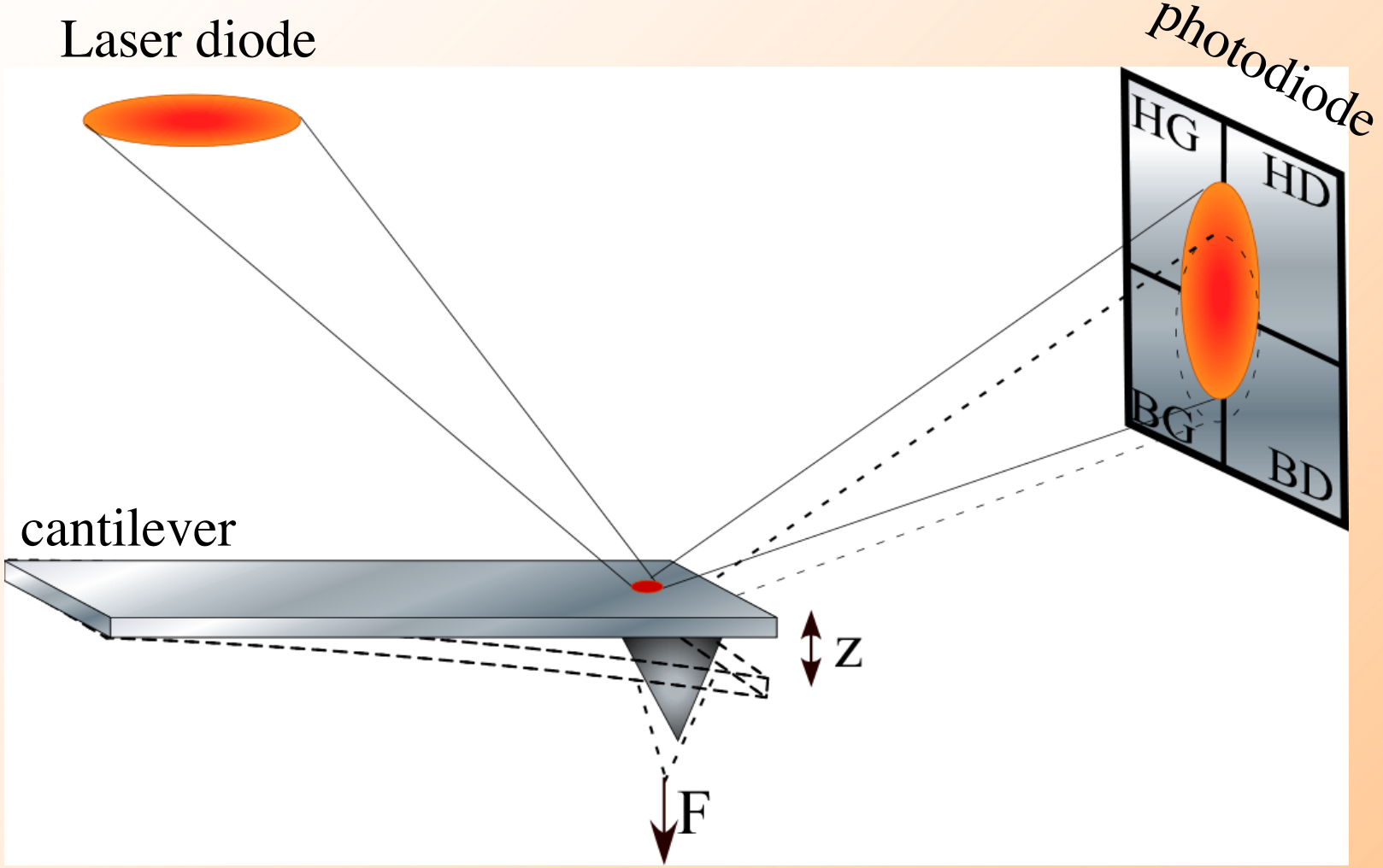

B) Deflection measurement

$$I_{mes} \propto A \frac{F}{k_c L}$$

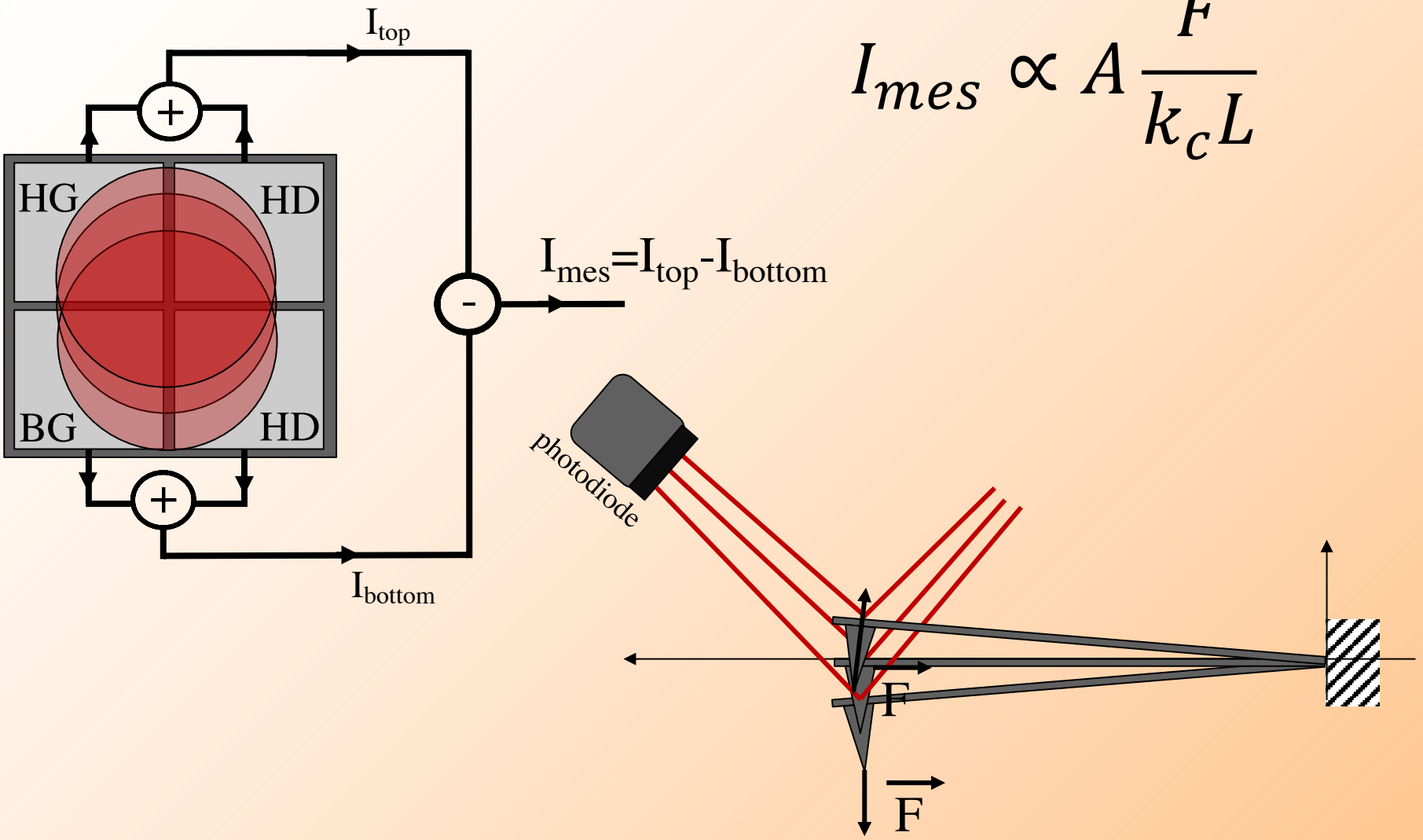

IV. Static mode

A) Force curve

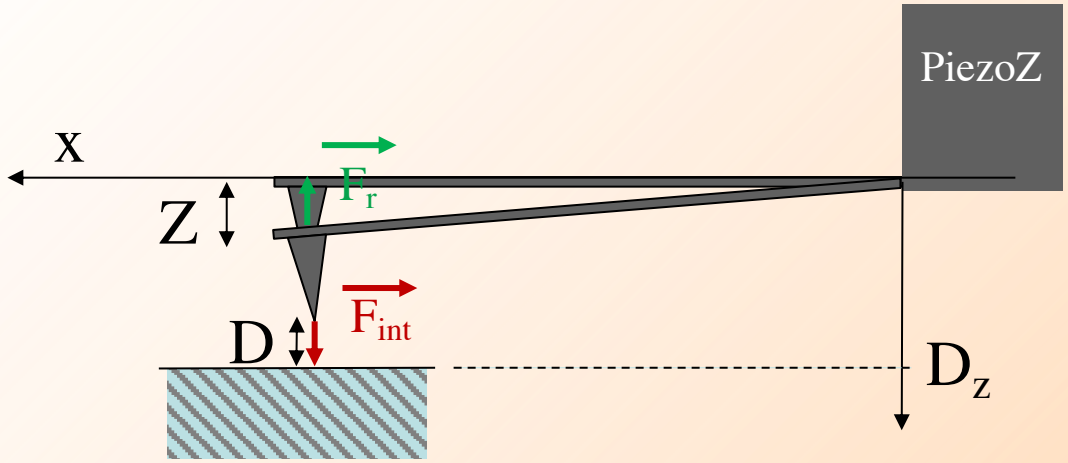

$$D_z = D + Z$$

Equilibrium of forces : $\overrightarrow{F_r} = \overrightarrow{F_{int}}$

$$-k_c Z = F^{s-p}(D)$$

$$-k_c(D_z - D) = F^{s-p}(D)$$

Line with k_c slope

DMT curve

Force curve $F(D_z)$

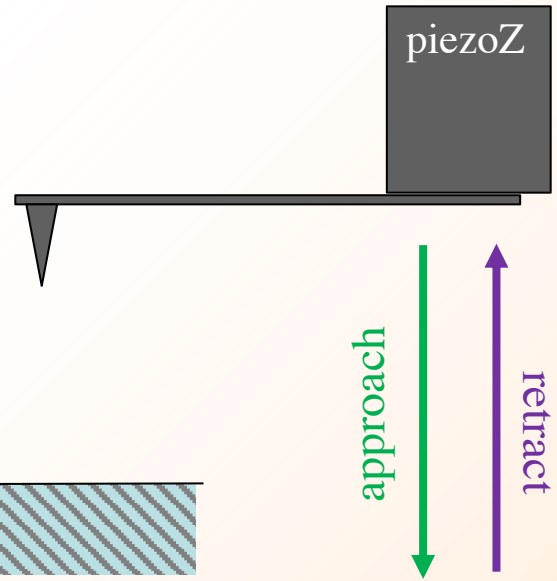

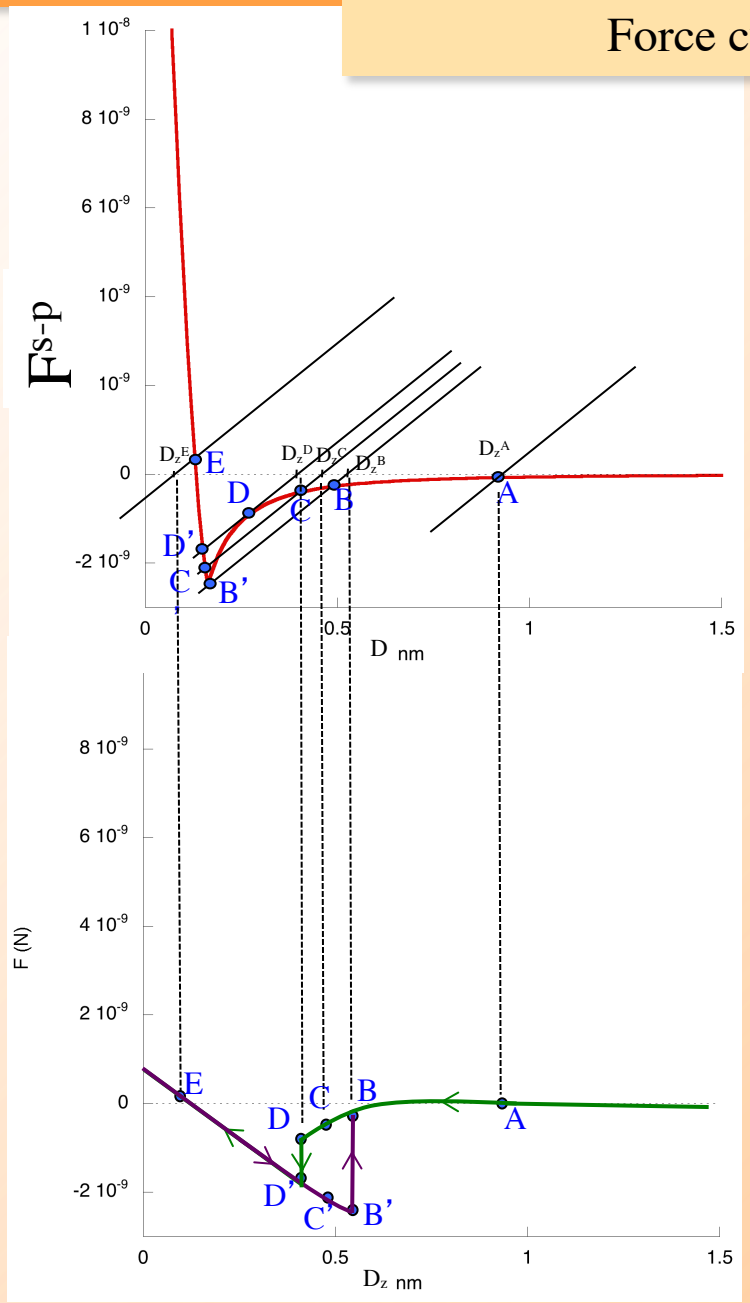

Force curveF(D_z)
On hard surface

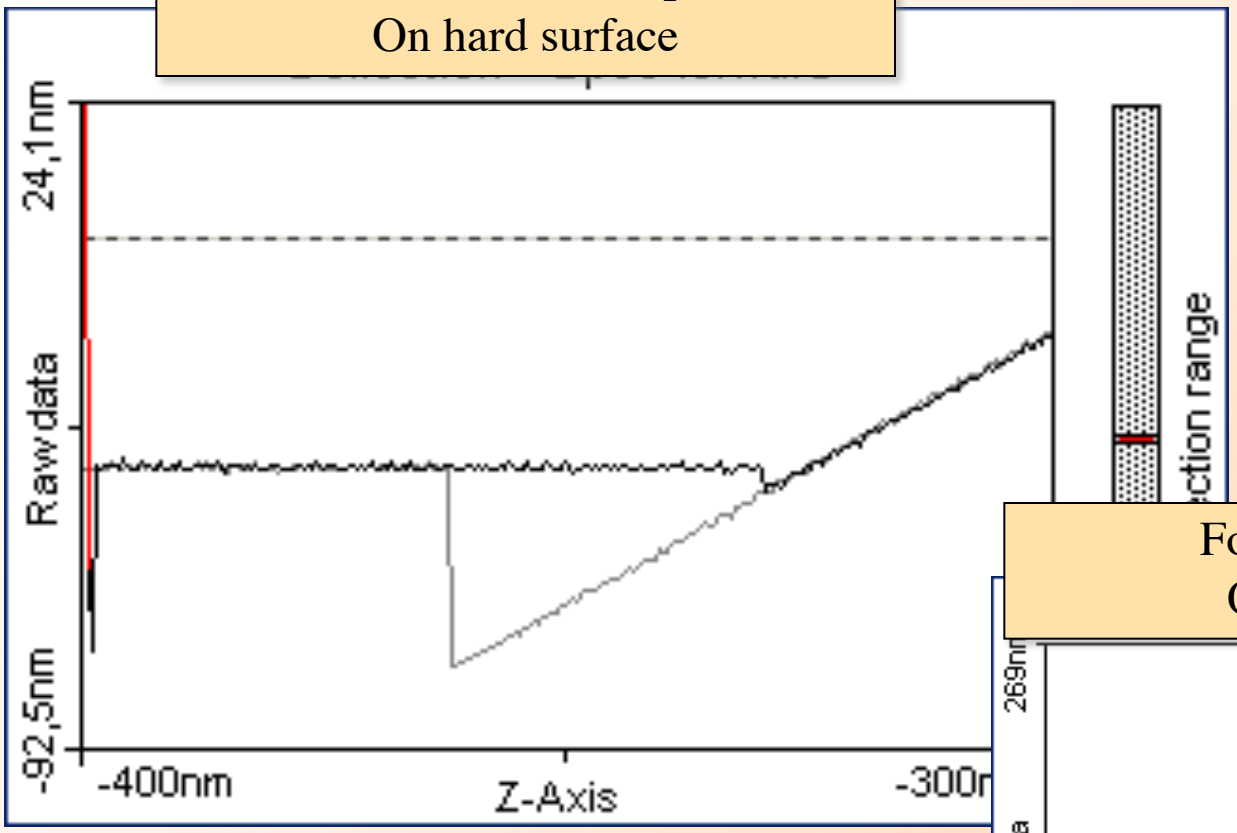

Force curve F(D_z)
On soft surface

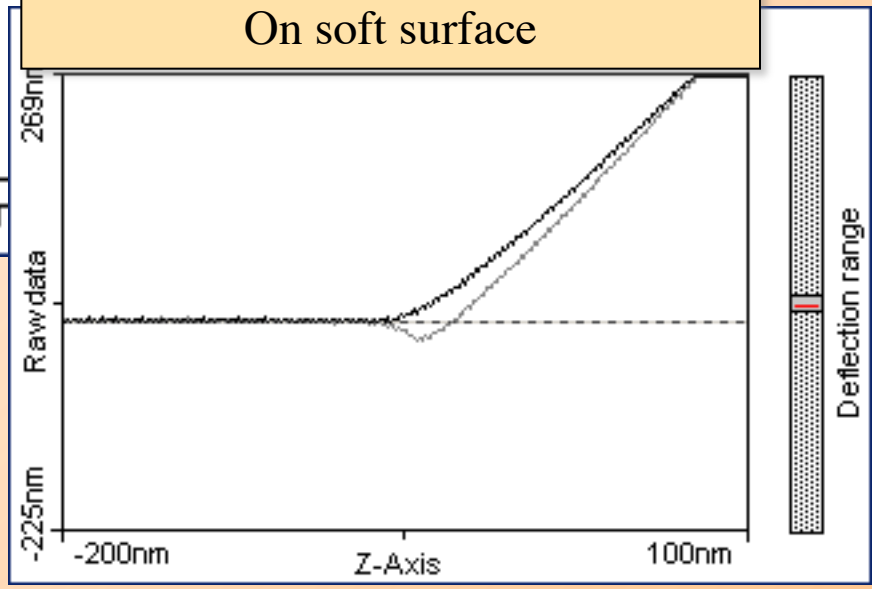

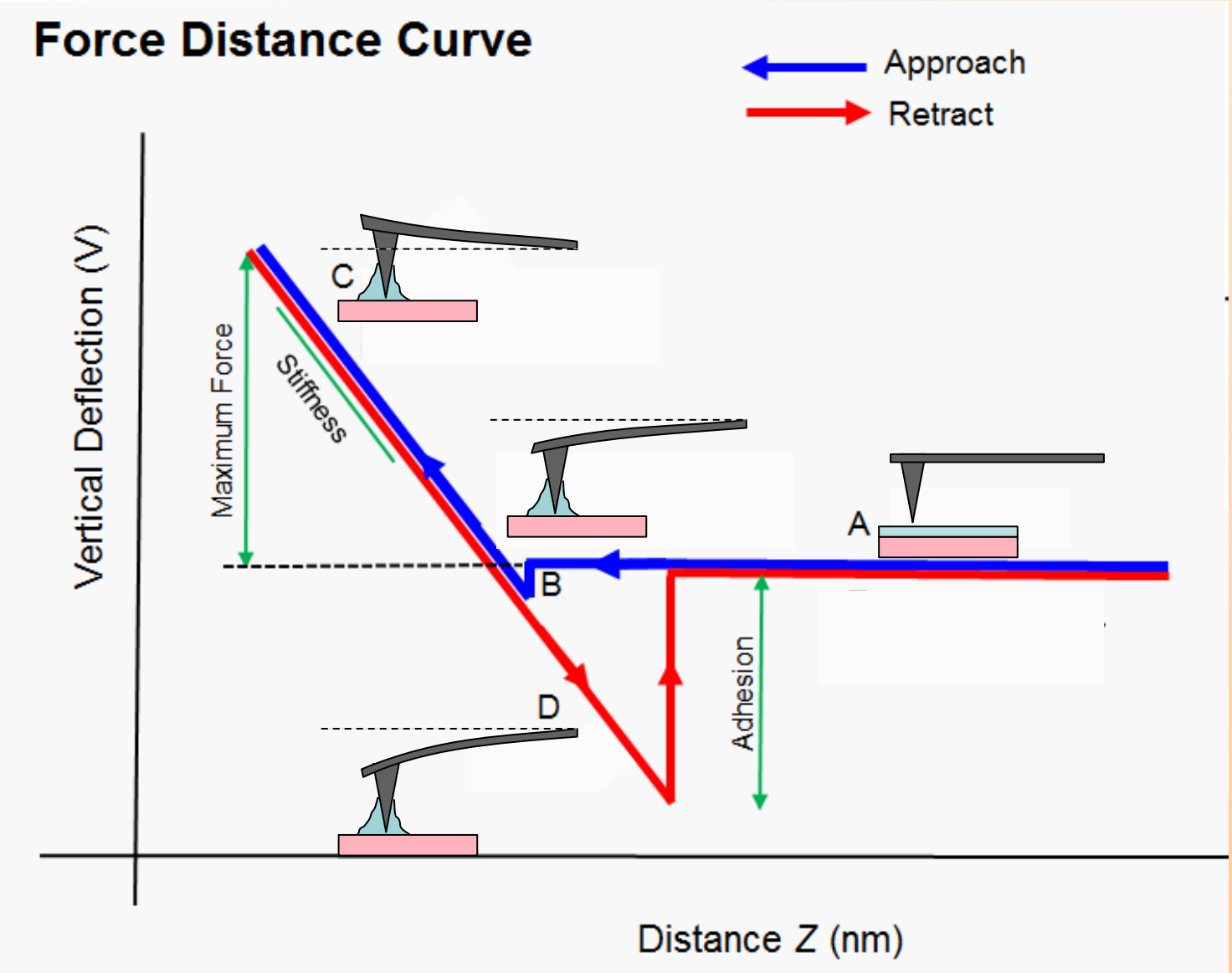
Force Distance Curve
Approach
Retract
Vertical Deflection (V)
Maximum Force
Stiffness
C
B
A
D
Adhesion
Distance Z (nm)

Application : Spectroscopy of single protein

Ubiquitin

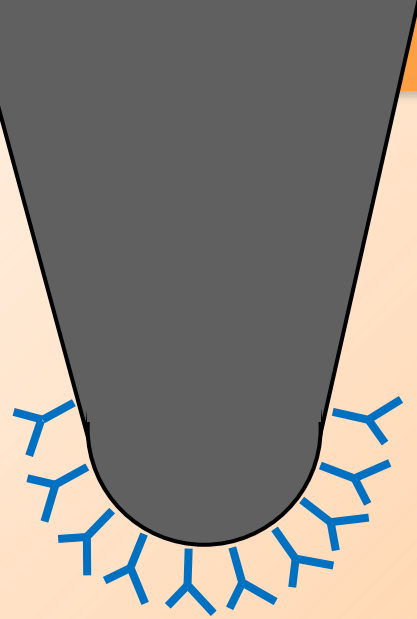

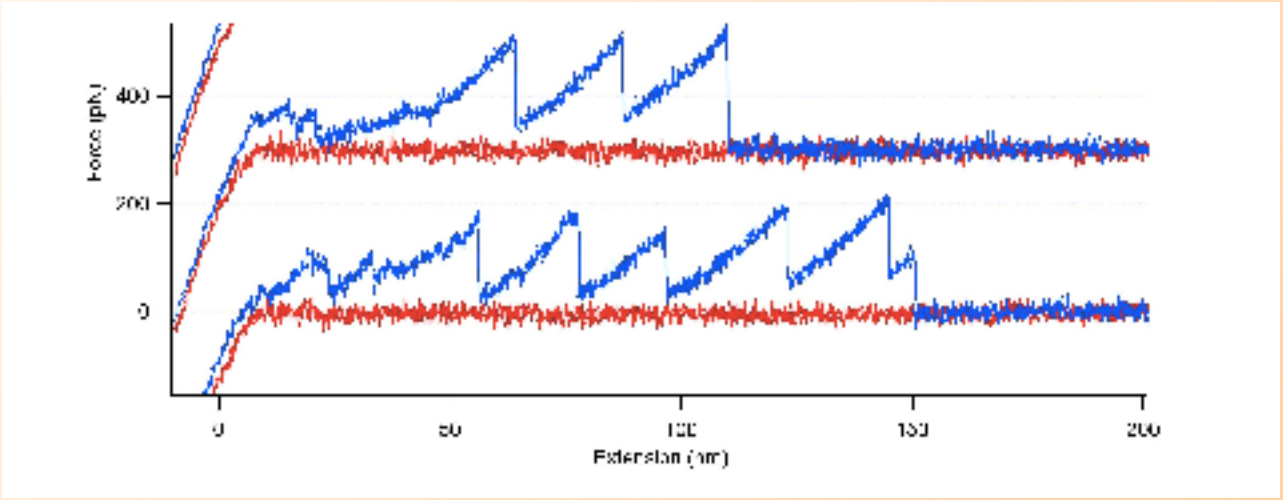

B) Imaging mode

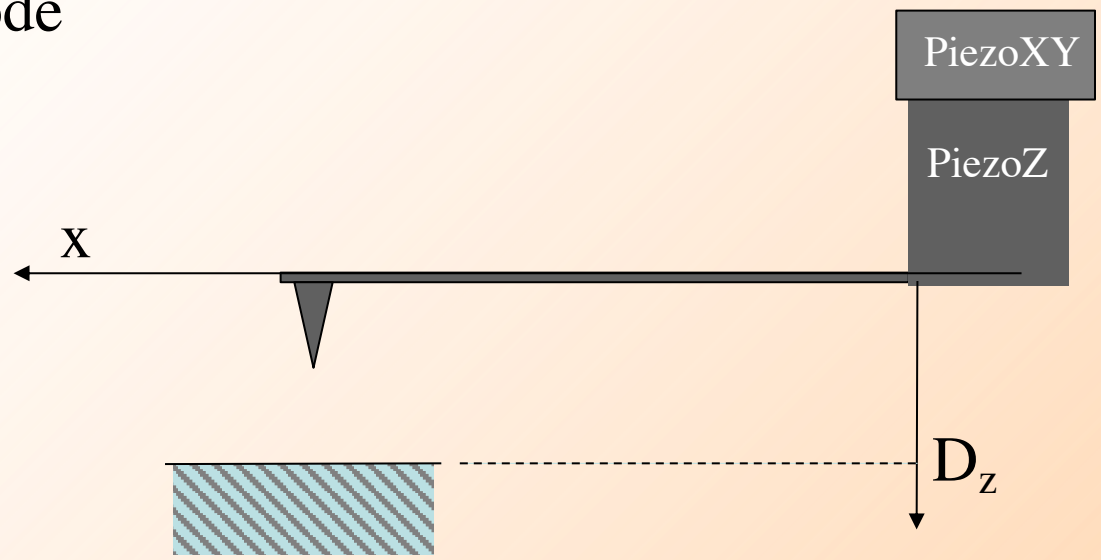

PiezoZ actuator : surface approach
PiezoXY actuators : scan of the surface in XY plane

Surface scanning:

1) Approach
2) Scanning X and Y

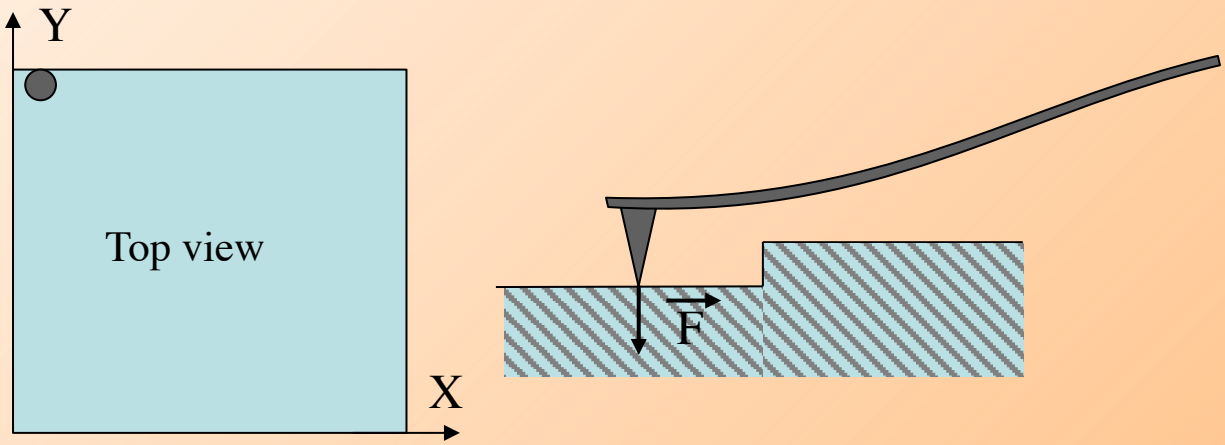

Constant force Imaging

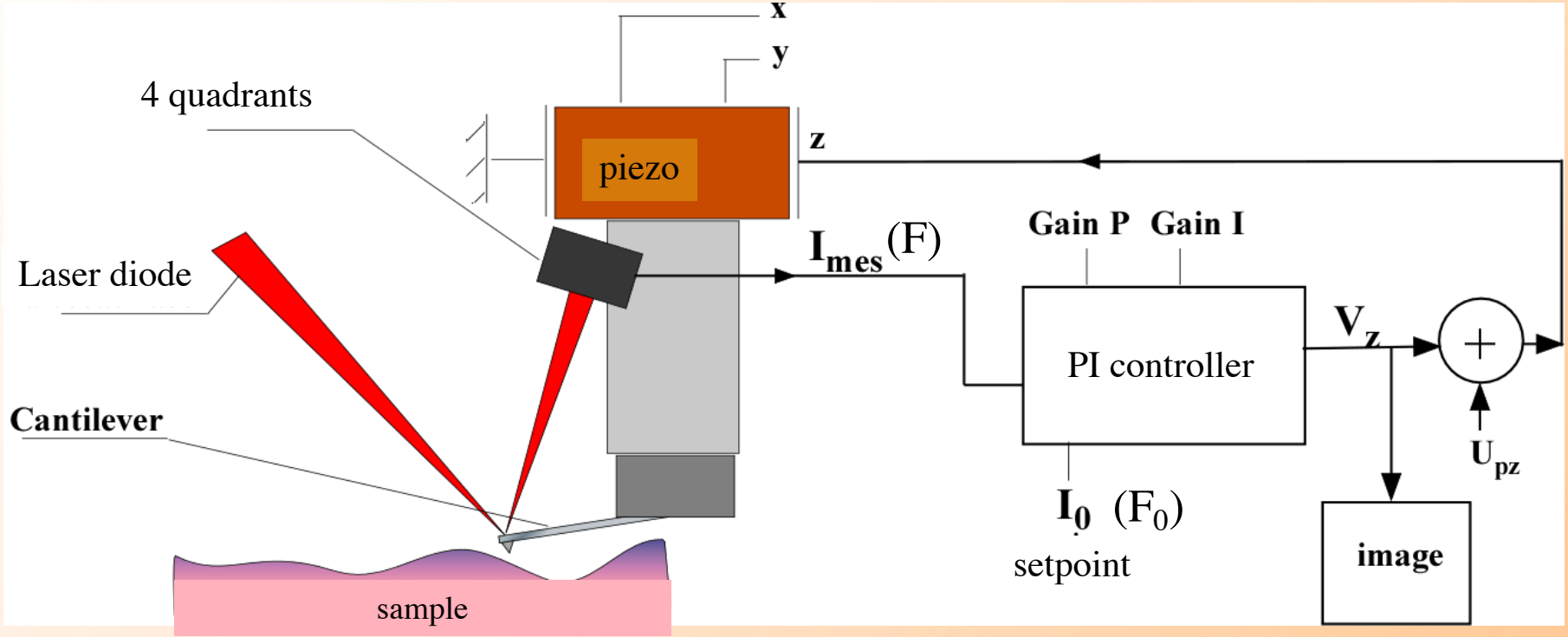

Modelling force constant imaging (F_0)

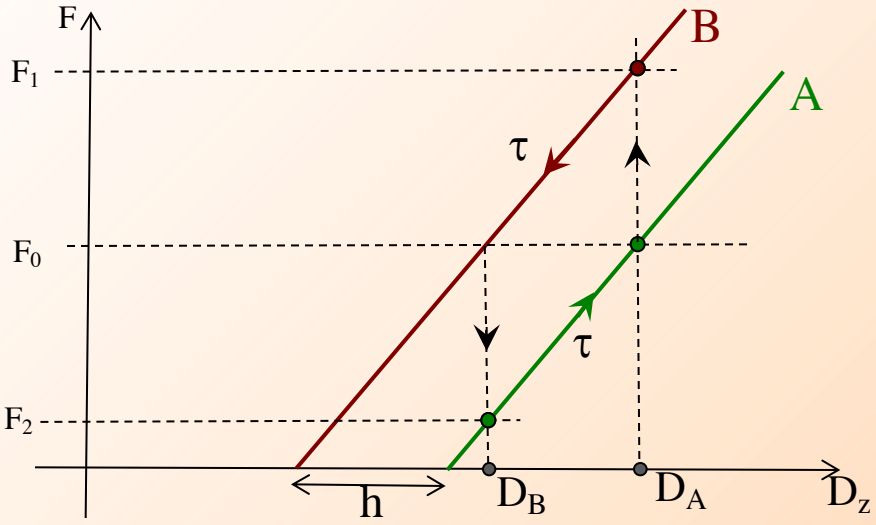

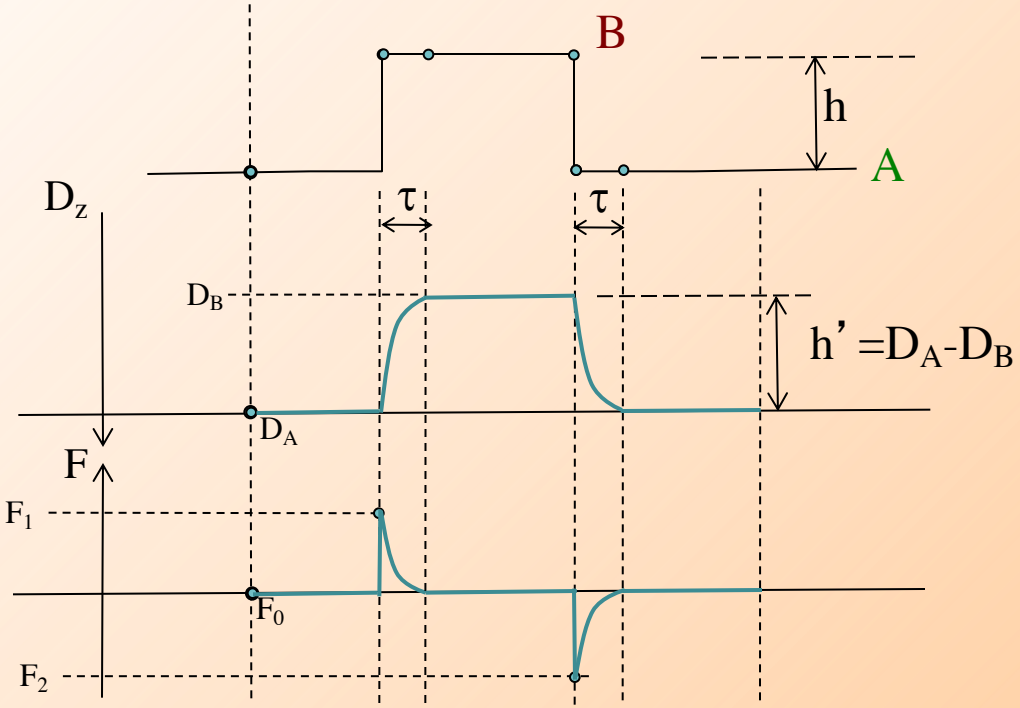

Contact mode images

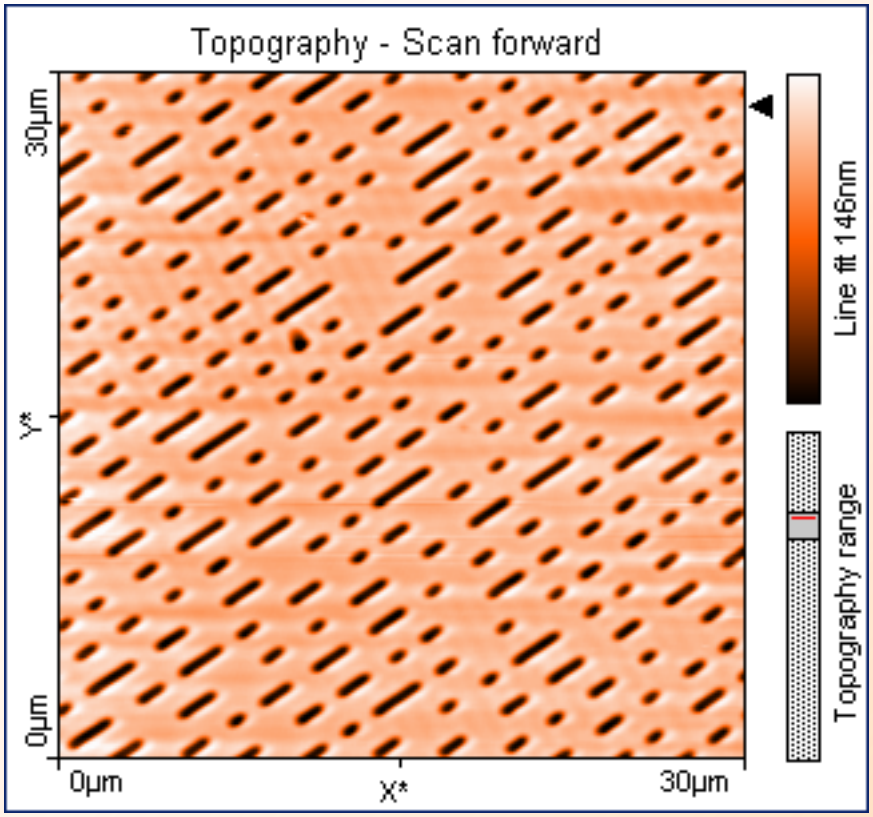

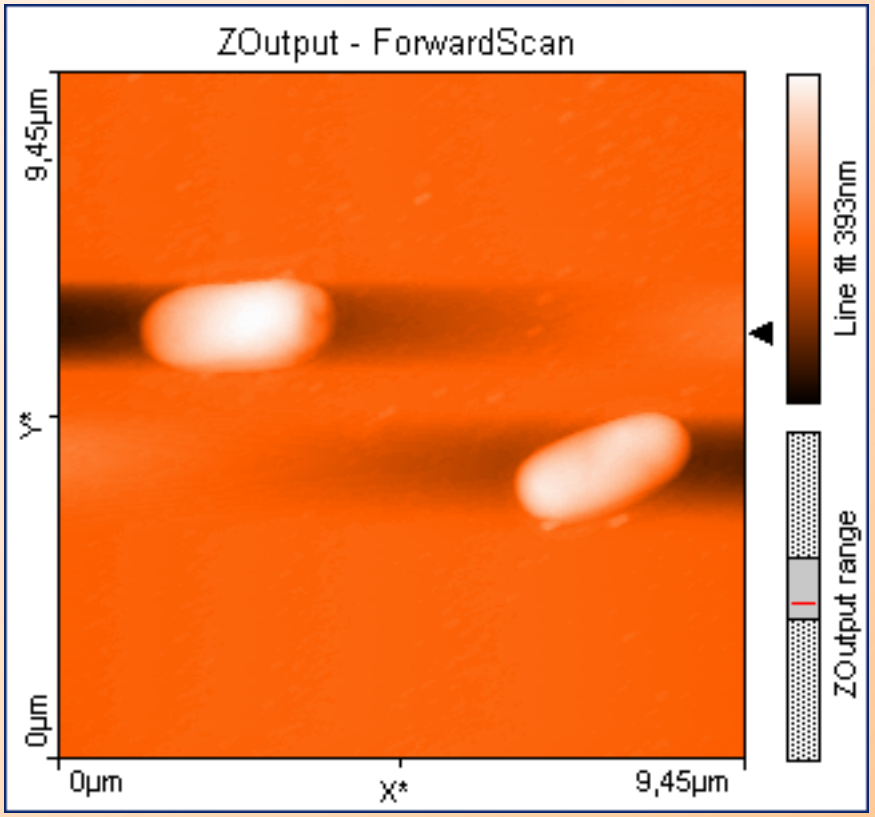

V. Dynamic mode (tapping)

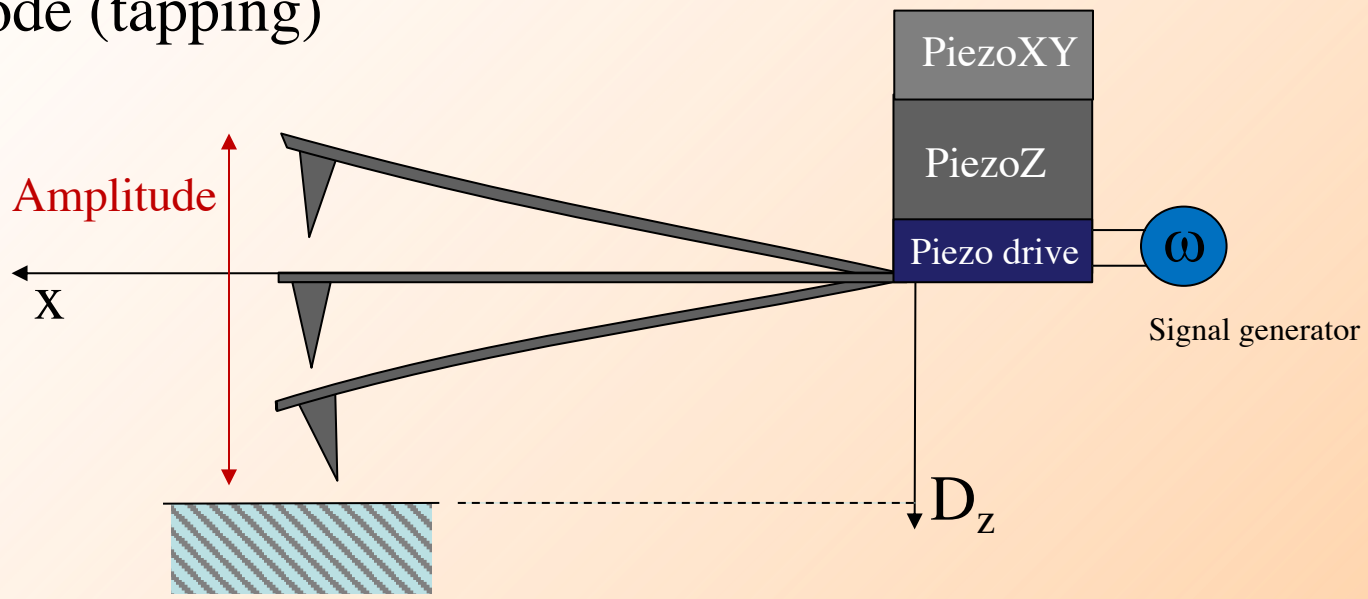

PiezoZ actuator : surface approach
PiezoXY actuators : scan of the surface in XY plane
Piezo drive : select the cantilever frequency of oscillation

Advantage : soft and fragile sample imaging
(no more shear effect during the scan)

CONTACT MODE

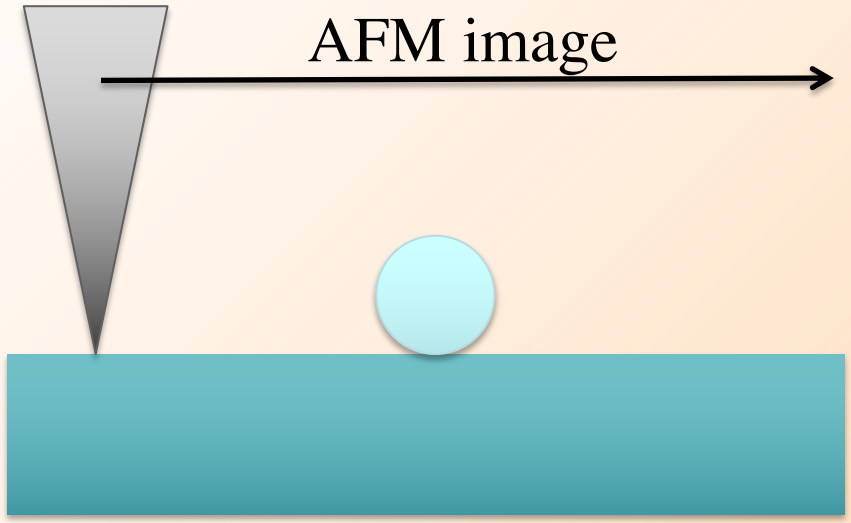

TAPPING MODE

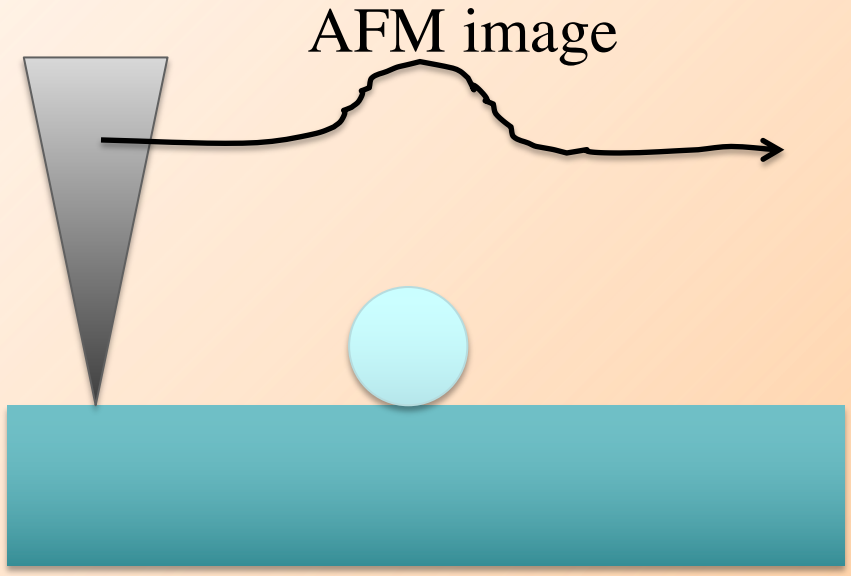

A) Cantilever modes

Euler-Bernouilli equation :

$$EI\frac{\partial z^4}{\partial x^4}+\kappa\frac{\partial z}{\partial t}+\rho S\frac{\partial z^2}{\partial t^2}=0$$

Solution :

$$z(x,t)=(Ae^{\beta x}+Be^{-\beta x}$$

$$+Ce^{i\beta x}+De^{-i\beta x})e^{i\omega t}e^{-\frac{\Gamma}{2}t}$$

with $\omega=\sqrt{\frac{EI}{\rho S}}\beta^2$ and $\Gamma=\frac{\kappa}{\rho S}$

frequency damping

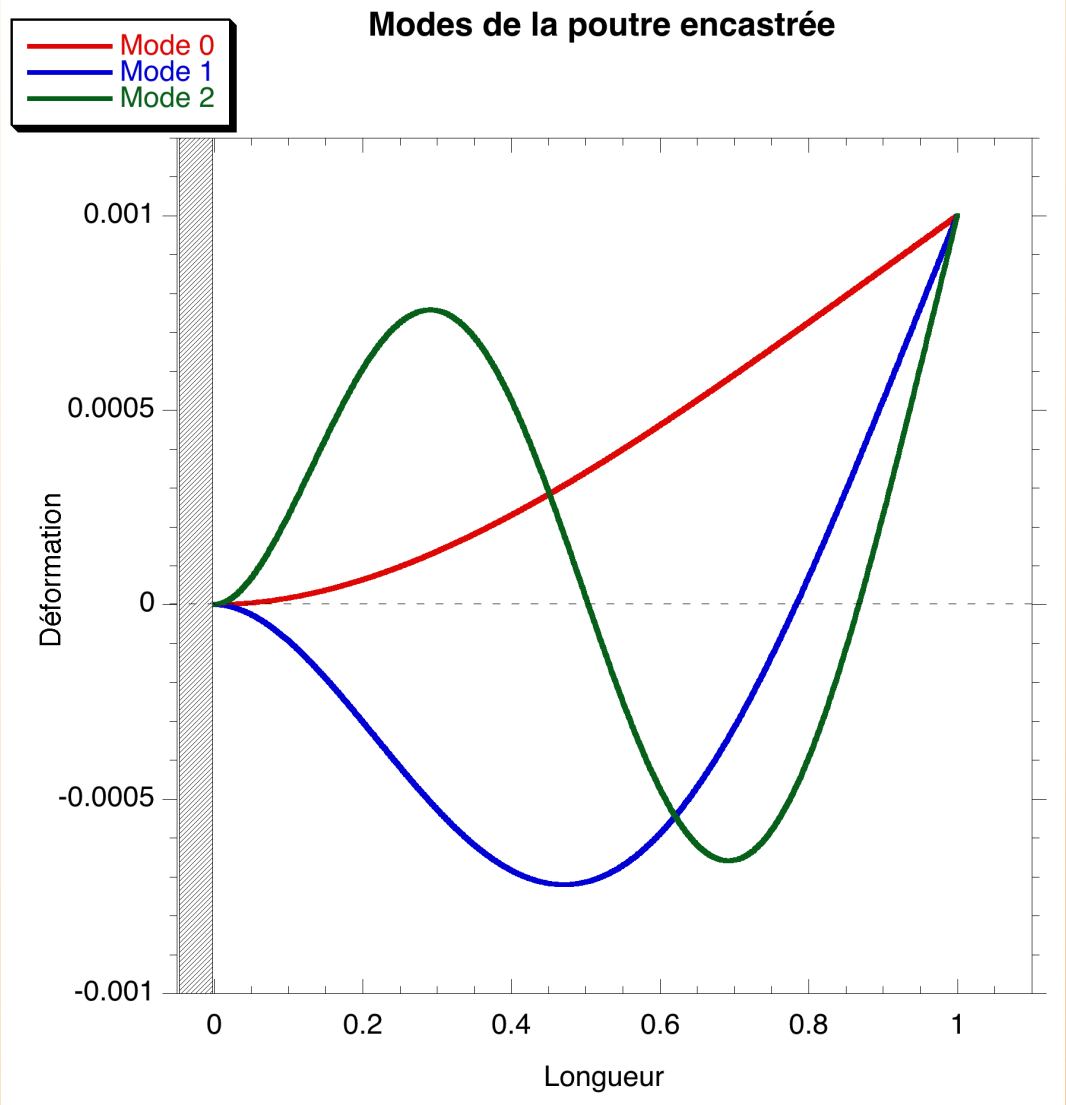

Euler-Bernouilli equation :

$$EI\frac{\partial z^4}{\partial x^4} + \kappa\frac{\partial z}{\partial t} + \rho S\frac{\partial z^2}{\partial t^2} = 0$$

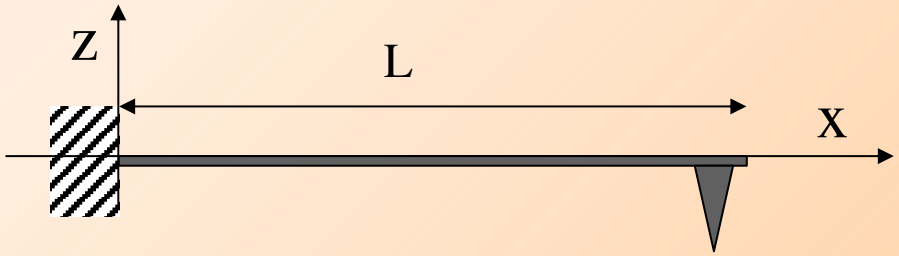

Boundaries conditions :

$$\begin{cases} z(0) = 0 \\ \left.\dfrac{\partial z}{\partial x}\right|_{x=0} = 0 \\ \left.\dfrac{\partial^2 z}{\partial x^2}\right|_{x=L} = 0 \\ \left.\dfrac{\partial^3 z}{\partial x^3}\right|_{x=L} = 0 \end{cases}$$

Eigenvalues (modes) equation of the cantilever :

$$1 + cos(\beta L)cosh(\beta L) = 0$$

Mode n	$\beta_n L$
0	1.8750
1	4.6941
2	7.8547

Dispersion equations

cantilever

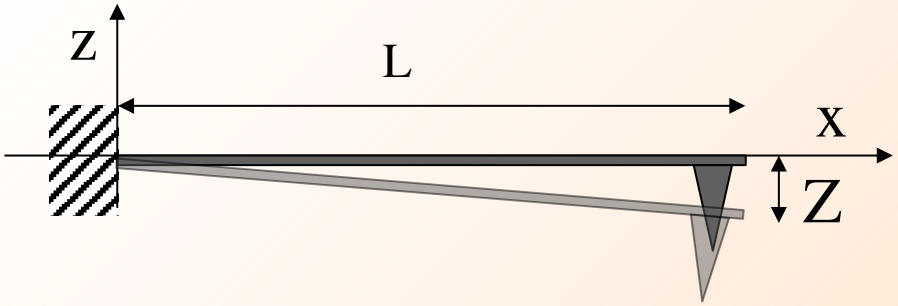

$$\omega_n = \sqrt{\frac{EI}{\rho S}}\beta_n{}^2$$

E, Young's modulus of the cantilever
I, area moment of inertia of the cantilever cross section
S, cross section : S=wt
ρ, cantilever density

mass-spring

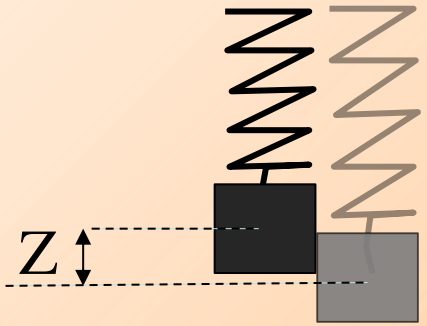

$$\omega_n = \sqrt{\frac{k_c}{m}}$$

k_c, spring constant
m, mass

Cantilever parameters :

$$\omega_n = \sqrt{\frac{EI}{\rho S}}{\beta_n}^2 \qquad k_c = \frac{3EI}{L^3} \qquad m = \rho S L$$

Each mode can be described by the mass-spring model.

$$\omega_n = \sqrt{\frac{k_c L^3}{3\rho S}}{\beta_n}^2 = \sqrt{\frac{k_c}{3m}}{\beta_n}^2 L^2 = \sqrt{\frac{k_c}{{m_n}^*}}$$

Where m_n^* is the mass of the mode

$${m_n}^* = \frac{3m}{(\beta_n L)^4}$$

Mode n	m_n^*
0	0.24267 m
1	0.00618 m
2	0.00079 m

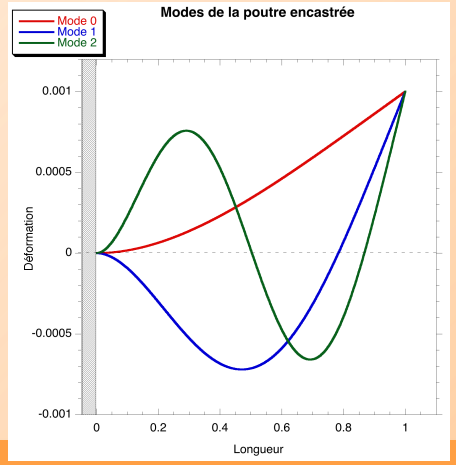

B) Motion equation of cantilever modes.

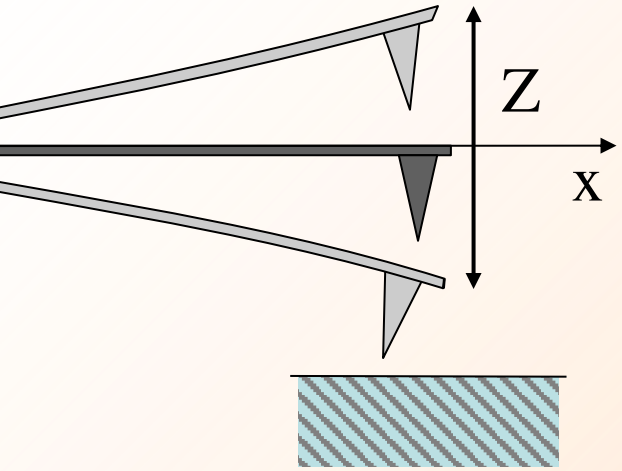

$$\frac{\partial^2 Z_n}{\partial t^2} + \Gamma \frac{\partial Z_n}{\partial t} + {\omega_n}^2 = 0$$

where $\omega_n = \sqrt{\frac{k_c}{{m_n}^*}}$, Γ damping, and Z_n the deflection of teh n^{th} modes

C) Motion equation of cantilever driven by a piezo.

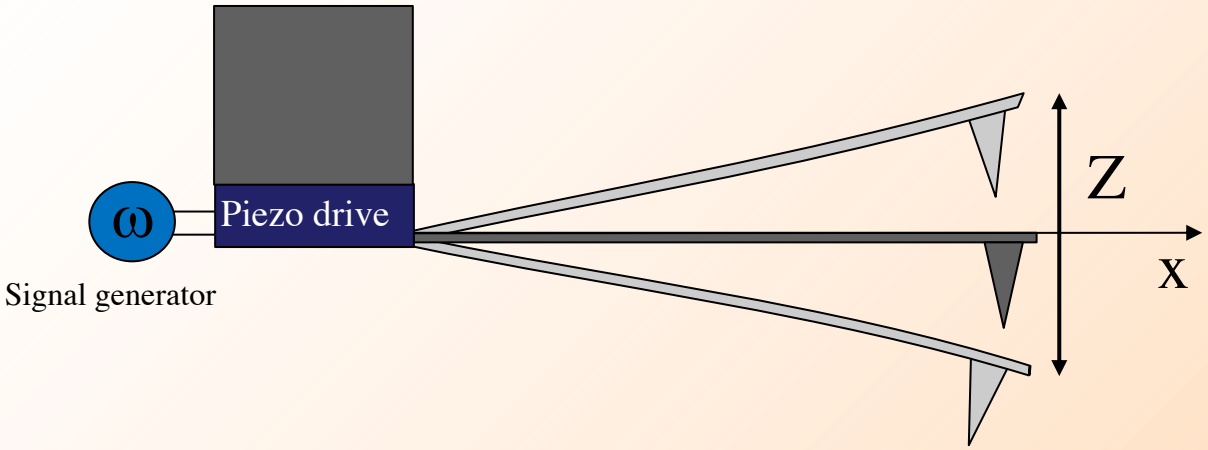

$$\frac{\partial^2 Z_n}{\partial t^2} + \Gamma \frac{\partial Z_n}{\partial t} + {\omega_n}^2 = \frac{F_{pz}}{{m_n}^*} e^{i\omega t}$$

where $\omega_n = \sqrt{\frac{k_c}{{m_n}^*}}$, Γ damping, and Z_n the deflection of teh n^{th} modes, F_{pz} force applied by the piezo

$$\frac{\partial^2 Z_n}{\partial t^2} + \Gamma \frac{\partial Z_n}{\partial t} + {\omega_n}^2 = \frac{F_{pz}}{{m_n}^*} e^{i\omega t}$$

Solution : $Z(t) = \tilde{A}(\omega) e^{i\omega t}$

$$-\omega^2 \tilde{A} + i\omega \tilde{A} \Gamma + {\omega_n}^2 \tilde{A} = \frac{F_{pz}}{{m_n}^*} \qquad \tilde{A}(\omega) = \frac{1}{{m_n}^*} \frac{F_{pz}}{{\omega_n}^2 - \omega^2 + i\omega\Gamma}$$

Solution : $Z(t) = \rho(\omega) e^{i(\omega t + \varphi(\omega))}$

$$\rho(\omega) = \frac{1}{{m_n}^*} \frac{F_{pz}}{\sqrt{({\omega_n}^2 - \omega^2)^2 + \Gamma^2 \omega^2}} \qquad \varphi = \tan^{-1}\left(\frac{\Gamma\omega}{\omega^2 - {\omega_n}^2}\right)$$

Exemple of 1rst mode of a cantilever

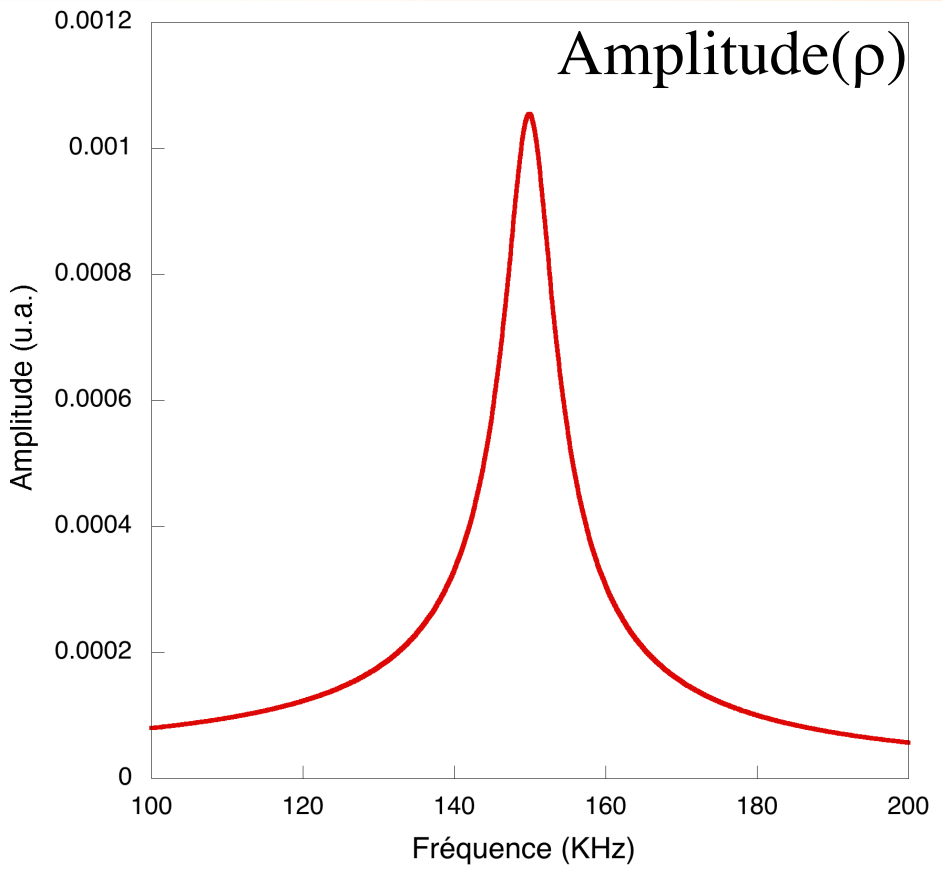

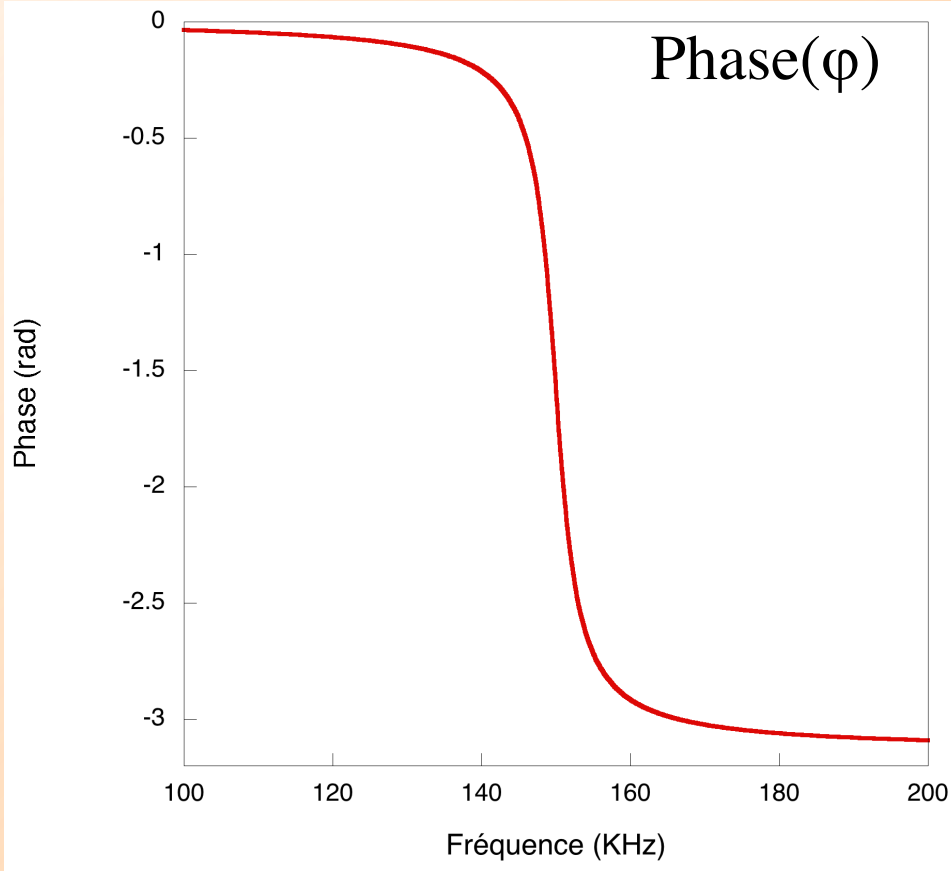

D) Motion equation of cantilever driven by a piezo and in interaction with the surface.

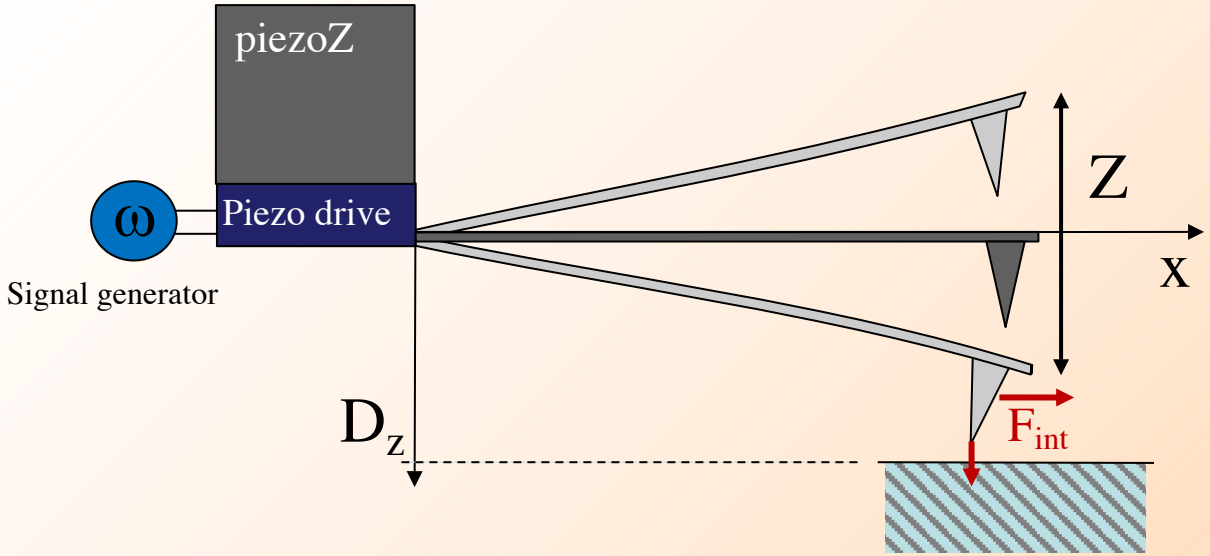

non linear term

$$\frac{\partial^2 Z_n}{\partial t^2} + \Gamma \frac{\partial Z_n}{\partial t} + {\omega_n}^2 = \frac{F_{pz}}{{m_n}^*} e^{i\omega t} + \frac{F_{int}(D_z - Z_n)}{{m_n}^*}$$

where $\omega_n = \sqrt{\frac{k_c}{{m_n}^*}}$, Γ damping, and Z_n the deflection of teh n^{th} modes, F_{pz} force applied by the piezo

Principle of least action (or principle of stationary action)

L is the Lagrangian of the mechanical system and defined by :

$$L = T - U$$

where T is the kinetic energy and U potential energy

S is the action defined as :

$$S = \int_{t_1}^{t_2} L(\dot{z}, z, t)dt$$

where t_1 and t_2 are 2 different times corresponding at 2 different positions of z.

The principle of least action is :

$$\delta S = 0 \; or \; \frac{\partial S}{\partial X_i} = 0$$

where X_i is the variables of the system

For a conservative system the equation of motion is found by :

$$\frac{d}{dt}\left(\frac{\partial L}{\partial \dot{z}}\right) - \frac{\partial L}{\partial z} = 0$$

Principle of least action in our case can be expressed as :

$$L(z,\dot{z},t) = \frac{1}{2}m^*\dot{z}(t)^2 - \left[\frac{1}{2}k_c z(t)^2 - z(t)F_{pz}cos(\omega t) + U_{int}\right] - \Gamma m^* z(t)\underline{\dot{z}(t)}$$

Kinetic energy

potential energy of the spring

potential energy of the piezo

Potential energy of tip-surface interaction

dissipation energy from the damping

Stationary solution can be written like :

$$z(t) = Acos(\omega t + \varphi)$$

variables of the system

We can rewrite the action as 3 different parts :

$$S = S_0 + S_{dissip} + S_{int}$$

where the action is calculated over a period of oscillation

$$S_0 = \int_0^{\frac{2\pi}{\omega}} \left(\frac{1}{2} m^* \dot{z}(t)^2 - \frac{1}{2} k_c z(t)^2 + z(t) F_{pz} cos(\omega t) \right) \mathrm{dt}$$

$$S_{dissip} = \int_0^{\frac{2\pi}{\omega}} \Gamma m^* z(t) \underline{\dot{z}(t)} \mathrm{dt}$$

$$S_{int} = \int_0^{\frac{2\pi}{\omega}} U_{int} \mathrm{dt}$$

Principle of least action tell us :

$$\begin{cases} \frac{\partial S}{\partial A} = 0 \\ \frac{\partial S}{\partial \varphi} = 0 \end{cases}$$

Equation becomes:

$$\begin{cases} cos\varphi = \dfrac{m^*}{F_{pz}} A({\omega_0}^2 - \omega^2) - \dfrac{\omega}{\pi F_{pz}} \dfrac{\partial S_{int}}{\partial A} \\ sin\varphi = -\dfrac{\Gamma m^*}{F_{pz}} \omega A \end{cases}$$

$$\omega_0 = \sqrt{\frac{k_c}{{m_n}^*}}$$

Pure attractive interaction

$$S_{int} = -\int_0^{\frac{2\pi}{\omega}} \frac{HR}{6\left(D - Acos(\omega t + \varphi)\right)^2} dt$$

$$\frac{\partial S_{int}}{\partial A} = \frac{HR\pi}{3\omega} \frac{A}{(D^2 - A^2)^{3/2}}$$

Pure repulsive interaction

$$S_{int} = -k_s \int_0^{\tau} (Acos(\omega t + \varphi) - D)^2 dt$$

k_s is contact spring constant

τ time of contact

$$\frac{\partial S_{int}}{\partial A} = -\frac{4\sqrt{2}}{3} \frac{k_s D}{\omega} \left(\frac{A}{D} - 1\right)^{3/2}$$

Resonance of the mode

Pure attractive interaction

$$u_{\pm} = \sqrt{\frac{1}{a^2} - \frac{1}{4Q^2}\left(1 \pm \sqrt{1 - 4Q^2\left(1 - \frac{1}{a^2} - \frac{\kappa_{nc}}{3(d^2 - a^2)^{3/2}}\right)}\right)^2}$$

Pure repulsive interaction

$$u_{\pm} = \sqrt{\frac{1}{a^2} - \frac{1}{4Q^2}\left(1 \pm \sqrt{1 - 4Q^2\left(1 - \frac{1}{a^2} + \frac{4\sqrt{2}}{3\pi}\kappa_c\left(1 - \frac{d}{a}\right)^{3/2}\right)}\right)^2}$$

$$u = \frac{\omega}{\omega_0} \quad d = \frac{D}{A_0} \quad a = \frac{A}{A_0} \quad A_0 = \rho(\omega_0) \quad Q = \frac{\omega_0}{\Gamma} \quad \kappa_c = \frac{k_s}{k_c} \quad \kappa_{nc} = \frac{HR}{k_c {A_0}^3}$$

Resonance behavior in function of the tip-surface distance

Attractive interaction

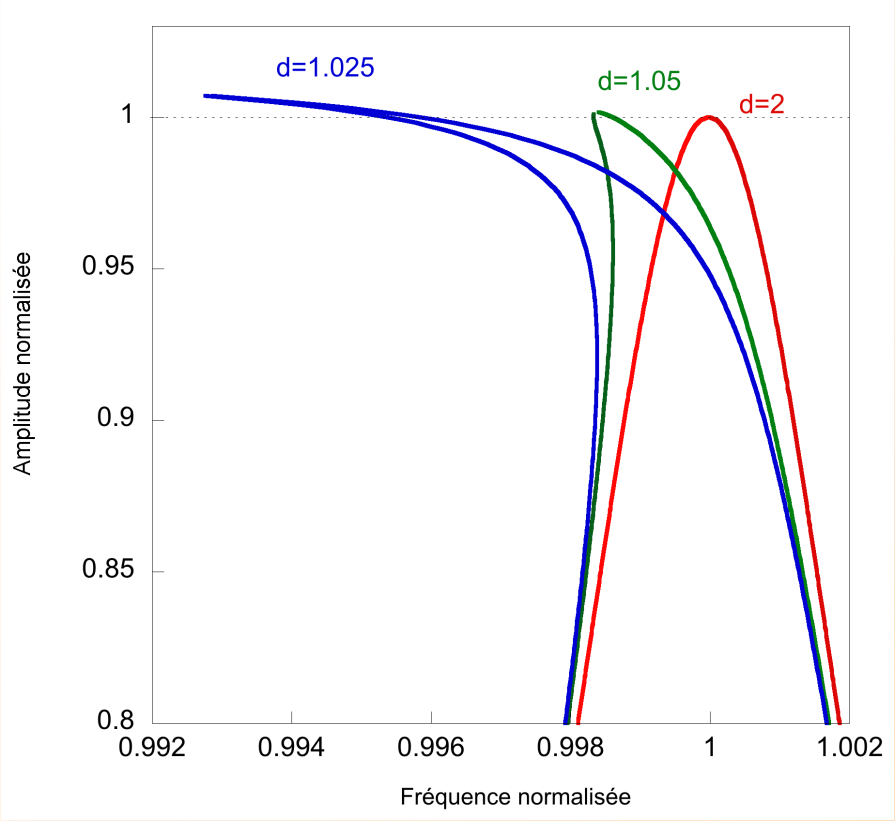

Repulsive interaction

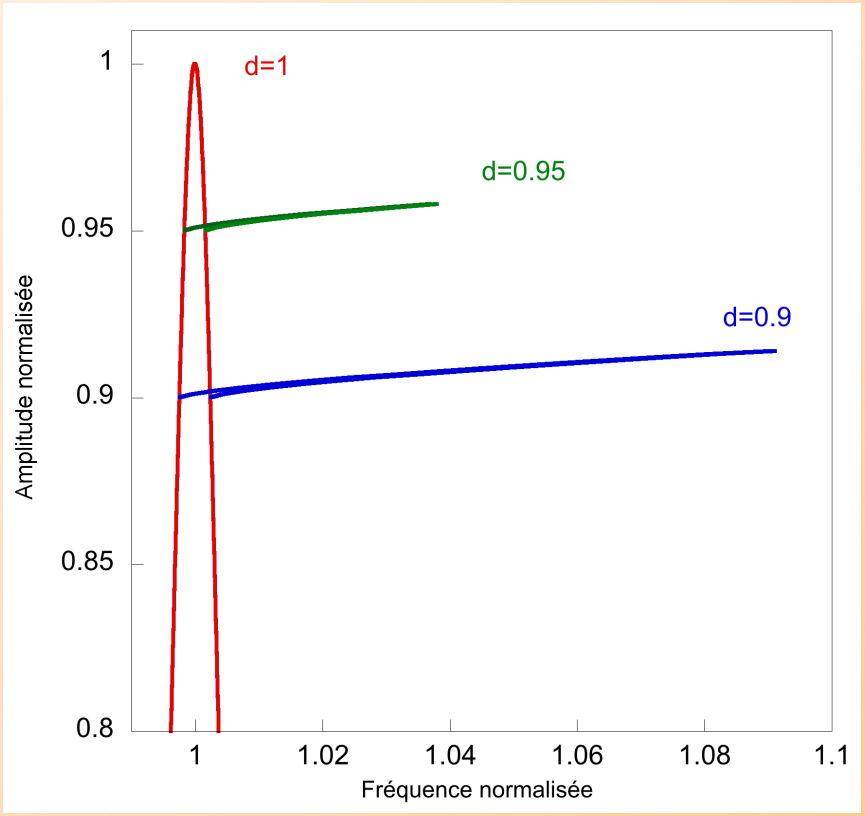

E) Approach-retract curve

$$Z(t) = A(\omega)cos\big(\omega t + \varphi(\omega)\big)$$

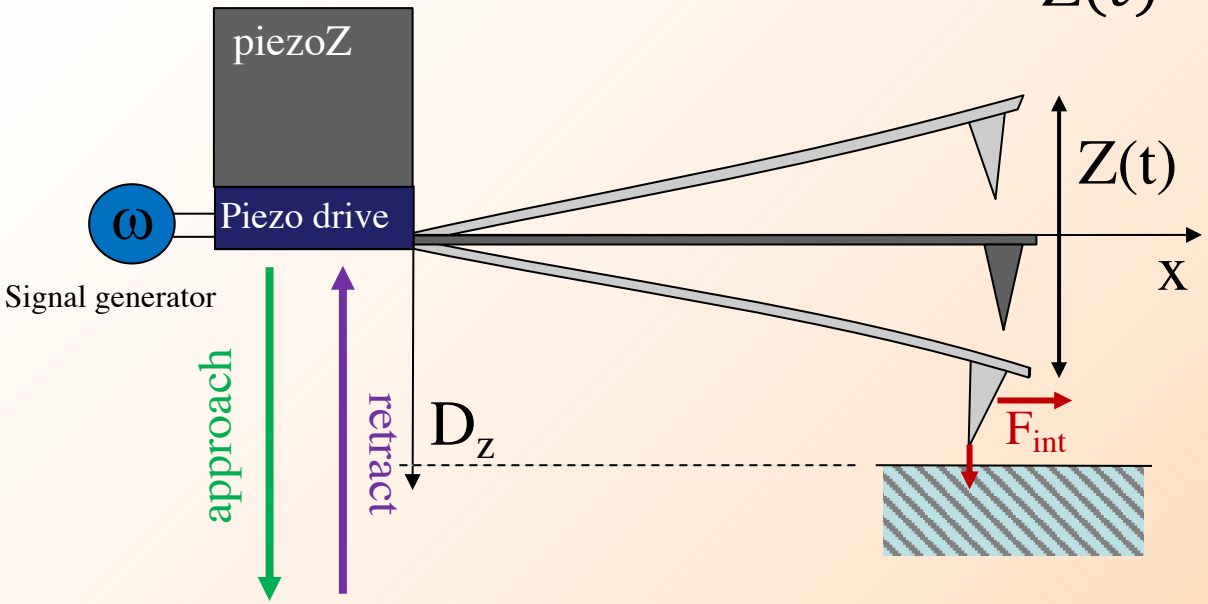

For a fixed ω (slightly off the resonance), analysis of Amplitude A(ω) and phase φ(ω) of the cantilever during the approach (increase of D_z) and retract (decrease of D_z).

Attractive interaction

$$\begin{cases} cos\varphi = Qa(1-u^2) - \dfrac{aQ\kappa_{nc}}{3(d^2-a^2)^{3/2}} \\ sin\varphi = -ua \end{cases}$$

$$d_{\pm} = \sqrt{a^2 + \left(\frac{Q\kappa_{nc}}{3\left(Q(1-u^2) \mp \sqrt{1/a^2 - u^2}\right)}\right)^{2/3}}$$

$$\varphi_{\pm} = \tan^{-1}\left(\frac{u}{Q(u^2-1) + \dfrac{Q\kappa_{nc}}{3\left(d_{\pm}{}^2 - a^2\right)^{3/2}}}\right)$$

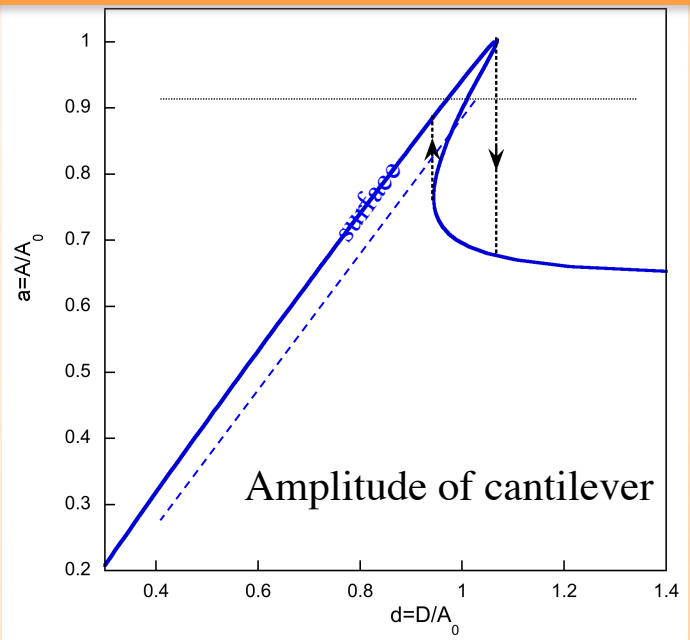

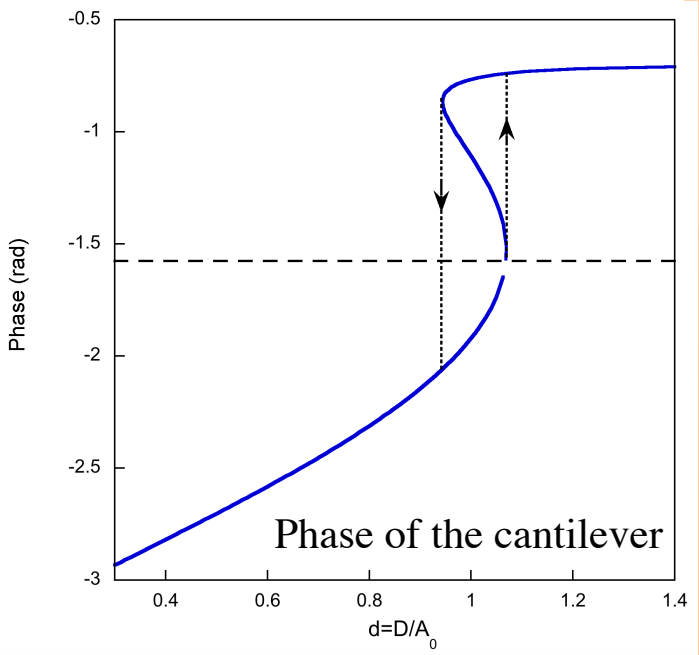

Repulsive interaction

$$\begin{cases} cos\varphi = Qa(1-u^2) + \dfrac{4\sqrt{2}}{3\pi} Q\kappa_c a \left(1 - \dfrac{d}{a}\right)^{3/2} \\ sin\varphi = -ua \end{cases}$$

$$d = a\left(1 - \left(\frac{3\pi}{4\sqrt{2}} \frac{Q(u^2-1) + \sqrt{1/a^2 - u^2}}{Q\kappa_c}\right)^{2/3}\right)$$

$$\varphi = \tan^{-1}\left(\frac{u}{Q(u^2-1) - \frac{4\sqrt{2}}{3\pi} Q\kappa_c \left(1 - \frac{d}{a}\right)^{3/2}}\right)$$

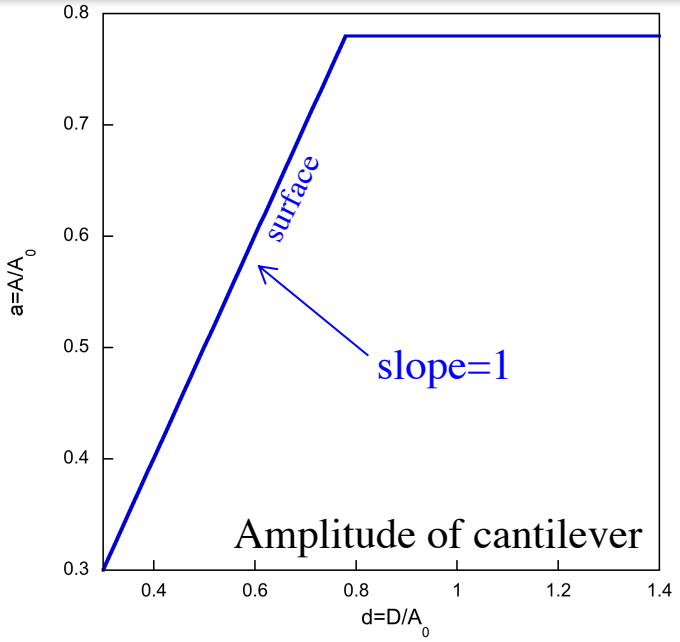

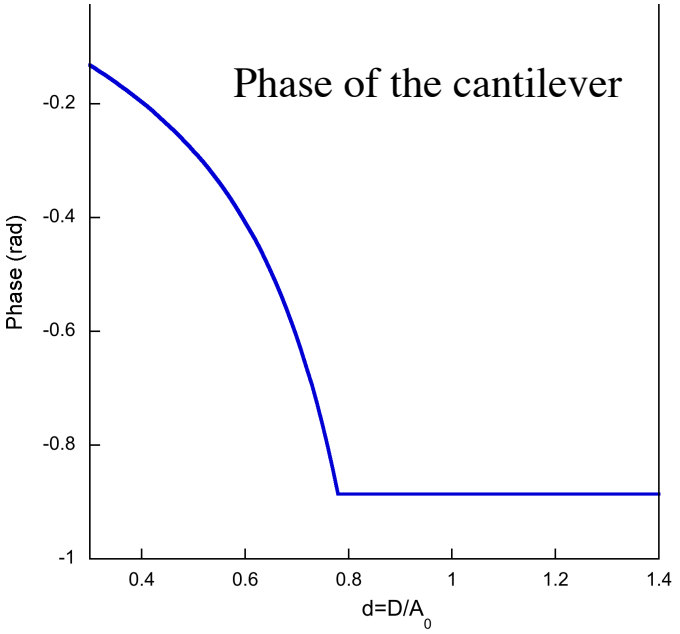

Modelling the amplitude and phase for different surface contact

Amplitude

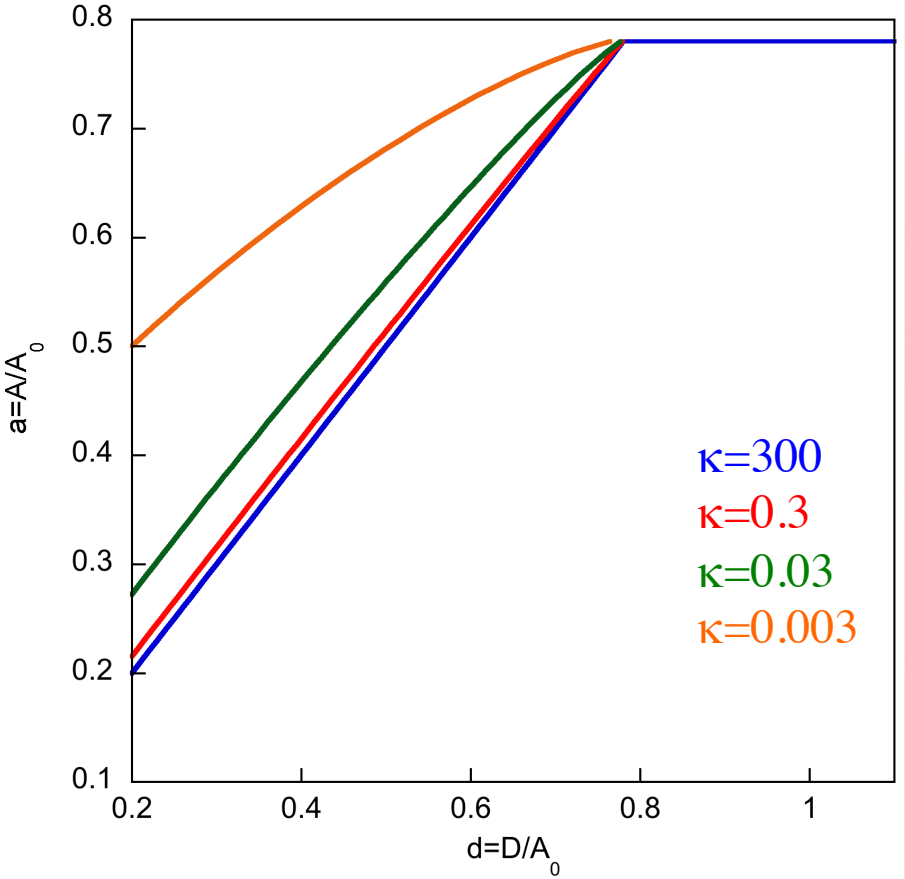

Phase

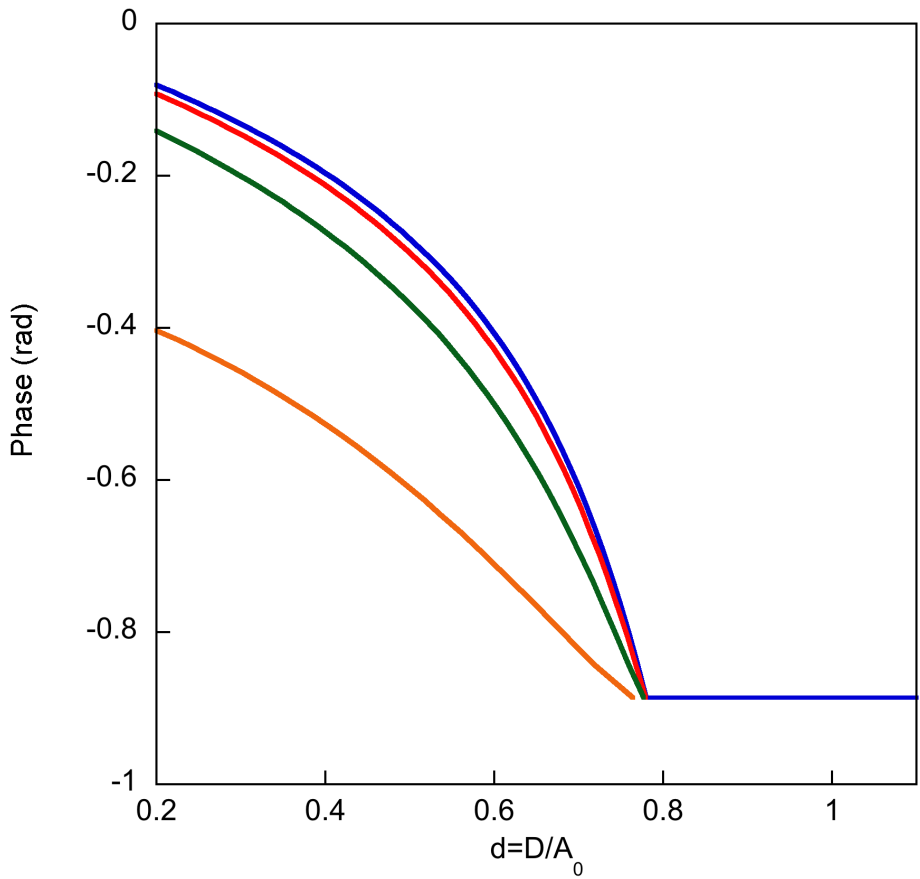

F) Imaging mode

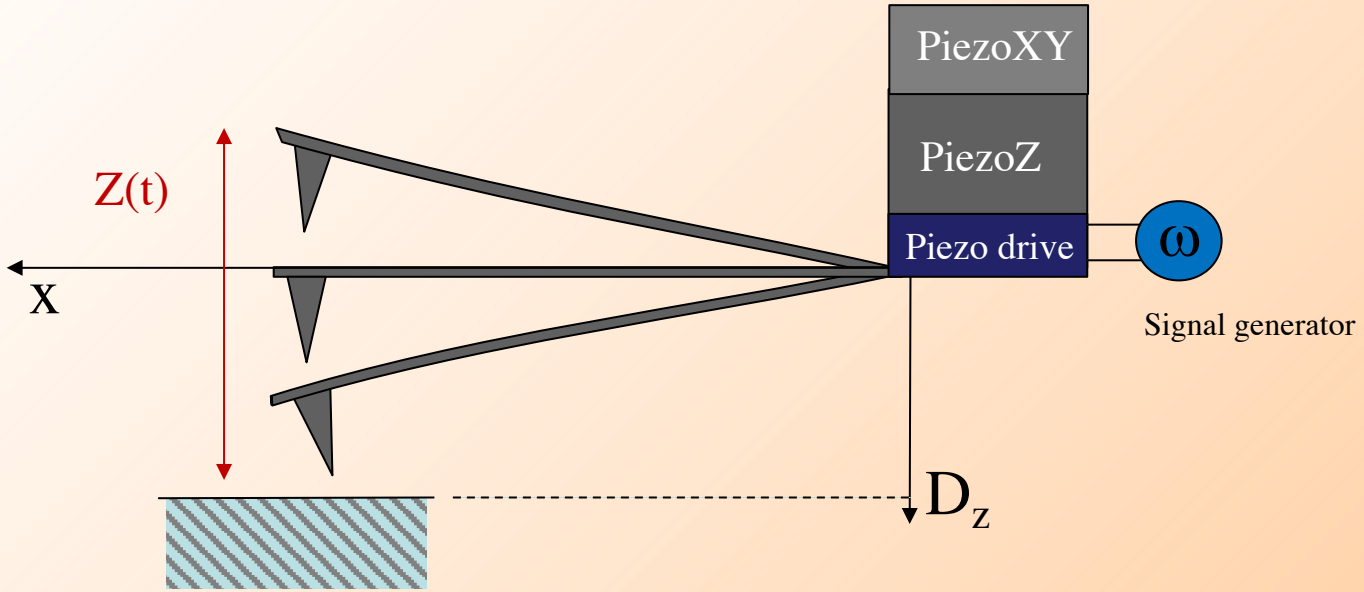

PiezoZ actuator : surface approach
PiezoXY actuators : scan of the surface in XY plane

Surface scanning:

1) Approach
2) Scanning X and Y

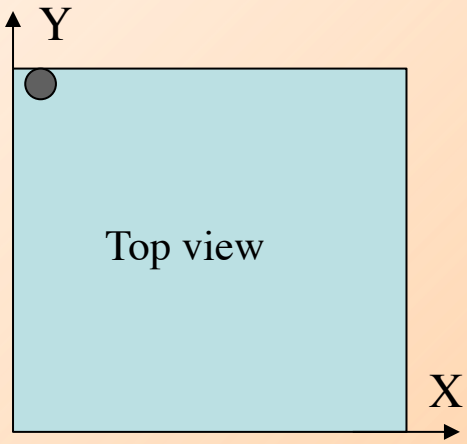

Constant amplitude imaging (tapping)

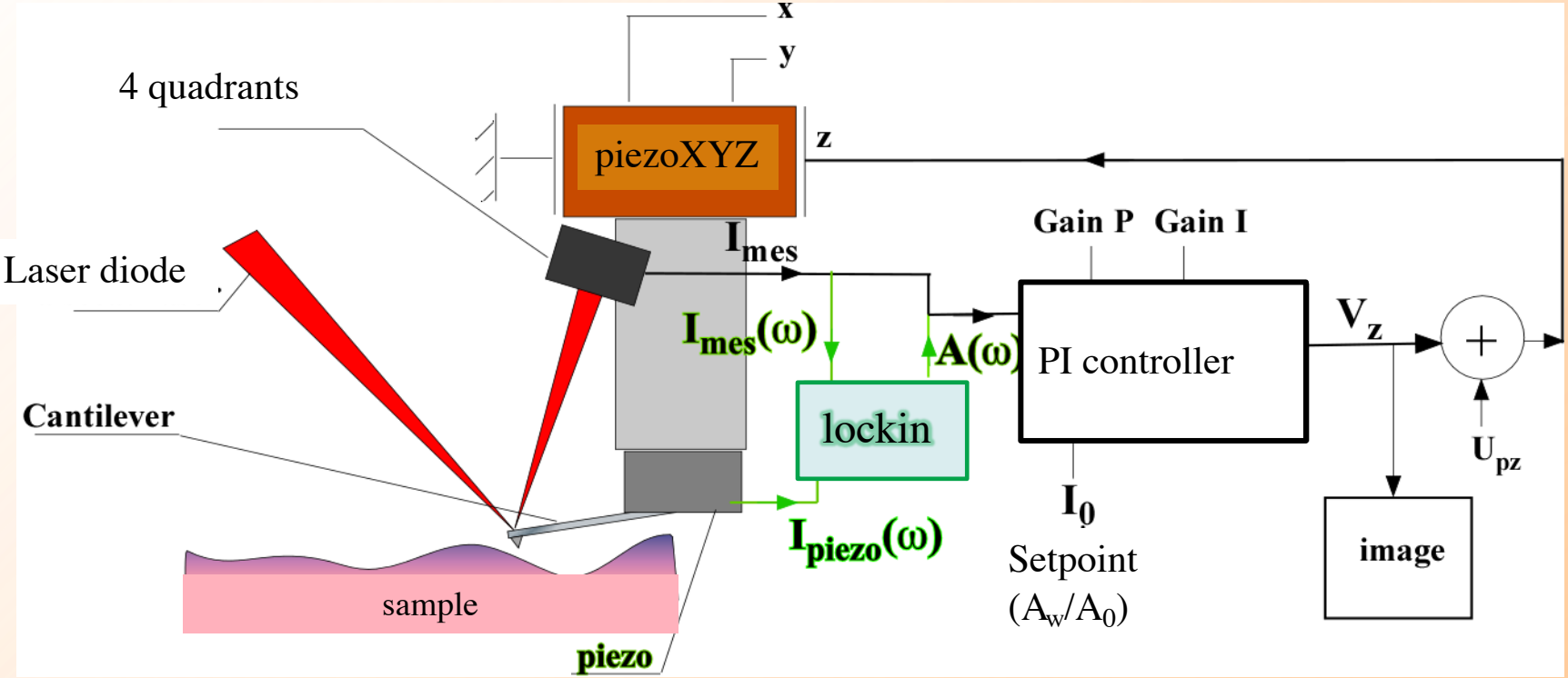

Tapping mode operation :

1) Use a cantilever for tapping mode with the first mode frequency around 70kHz-400kHz.

2) Detecting of the resonance of mode. Measurement of the Amplitude in function of the frequency of the piezo driver.

3) Selecting the working frequency (A_{free})

4) Selecting the setpoint for imaging (A_w/A_0)

5) Approaching the surface until reaching the setpoint (A_w/A_0)

6) Scan in X and Y axis keeping the amplitude constant (setpoint) recording the variation of V_z as the topography image

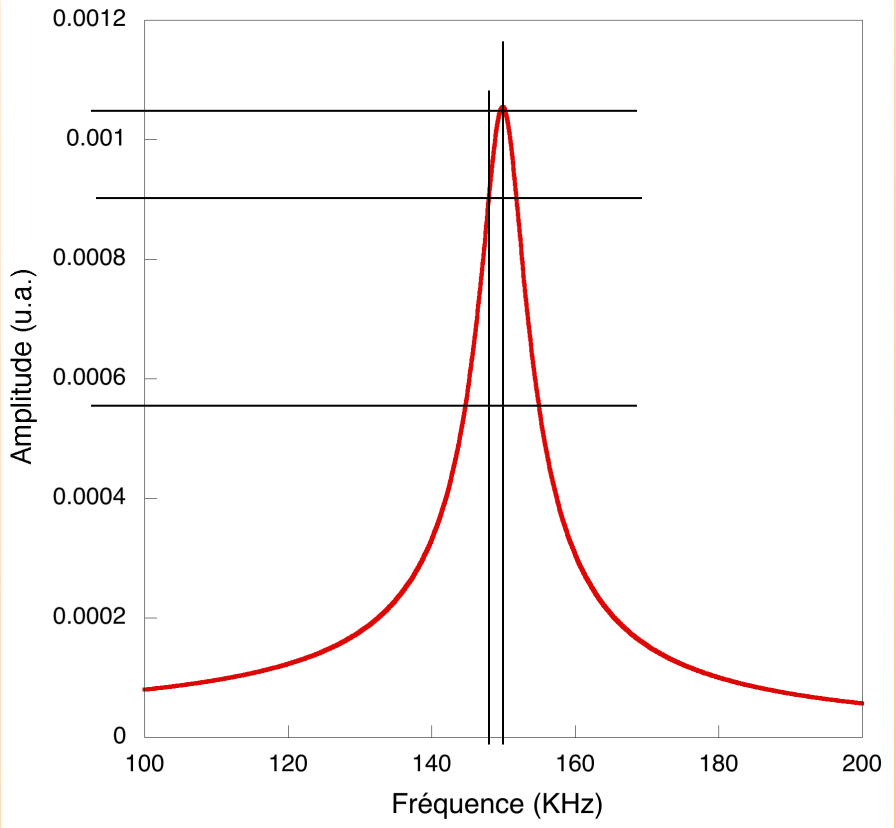

Tapping mode imaging

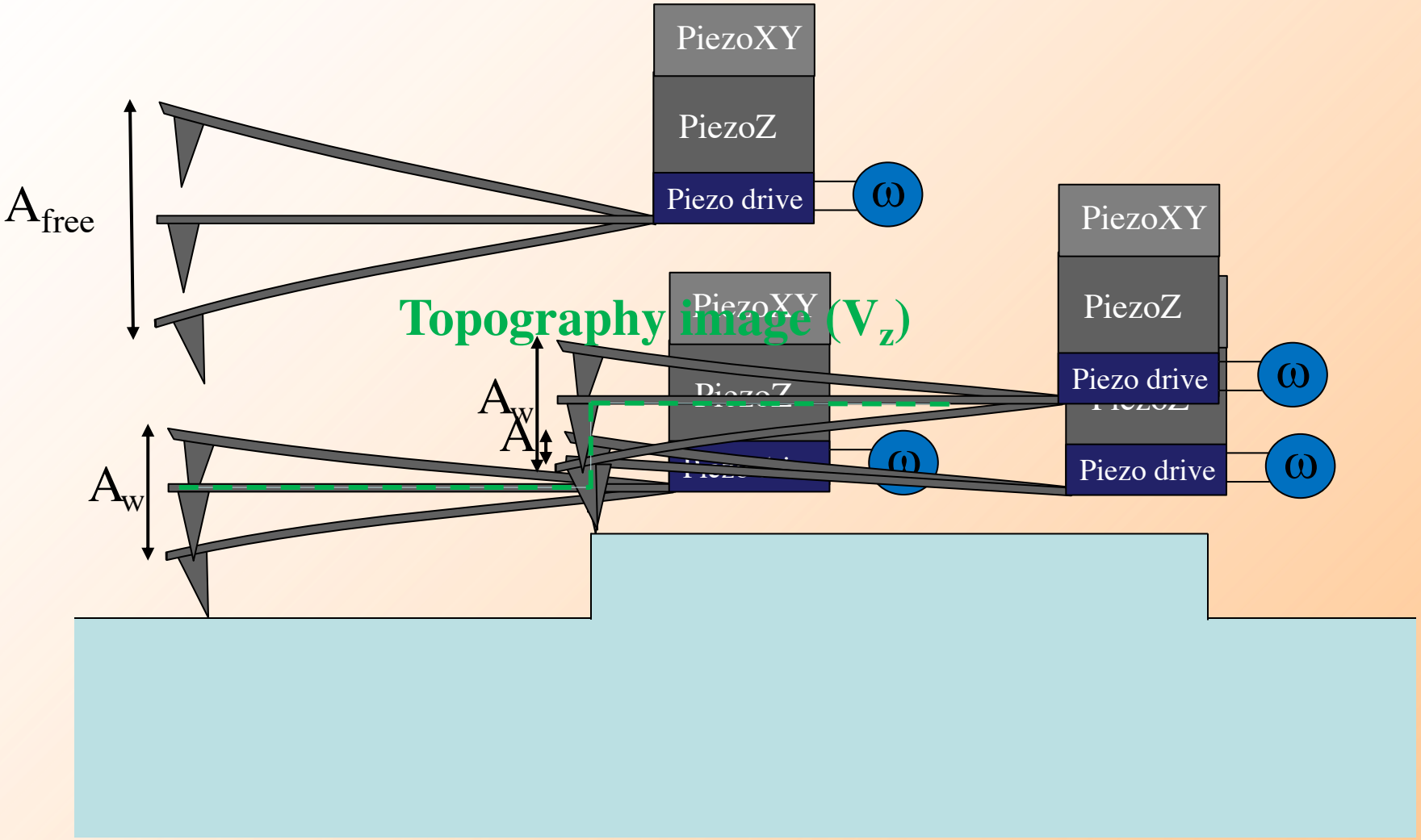

Image AFM en mode dynamique

ADN (100nm x 100 nm)

Tip effect example

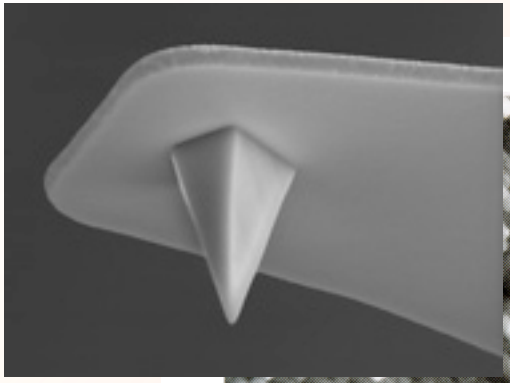

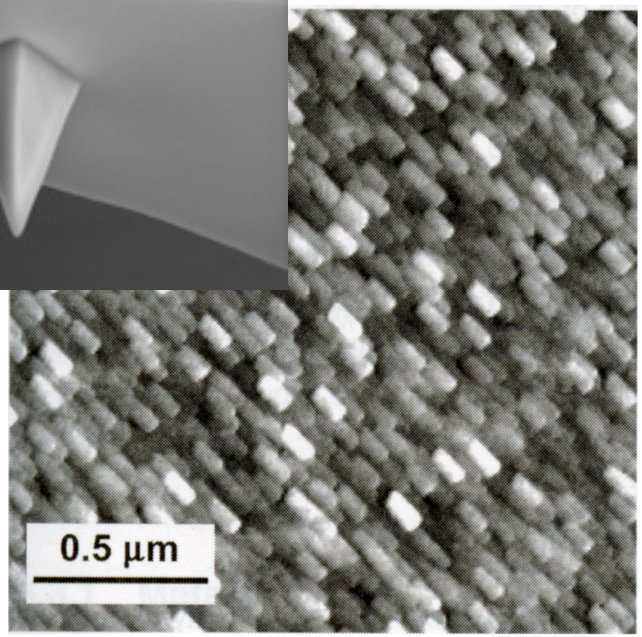

a

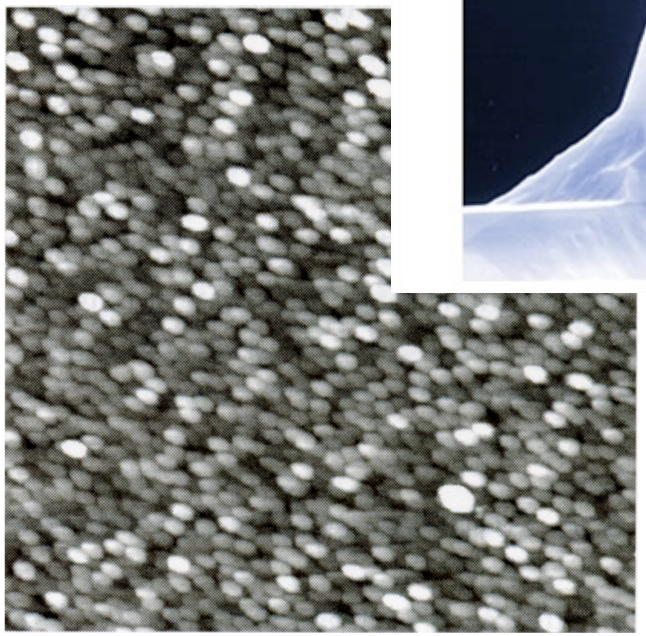

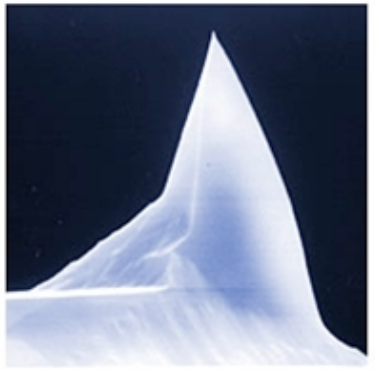

b

Contact AFM images of the same area of a (001) oriented TiO_2 thin film deposited on an $Al_2O_3(10\bar{1}0)$ substrate by sputtering. **a**, AFM image aquired with a pyramidal Si_3N_4 tip (Digital Instruments). **b**, Image acquired with a conical, etched Si tip (Digital Instruments). Both images are on the same scale and in the same surface orientation. In both cases, when the sample was rotated, the orientation of the surface features did not change. Clearly, the tip shape is convoluted into the surface morphology in both images.

A) Vertical sensitivity

Goes to 30pm to 300pm, strongly dependent on the AFM system, vibration isolation table and environment.

B) Lateral resolution

Strongly dependent on the AFM system and the tip radius:
can go from sub-nanometer up to 10 nm resolution

OTHER AFM OPERATING MODES

AFM in fluid

Contact and tapping mode

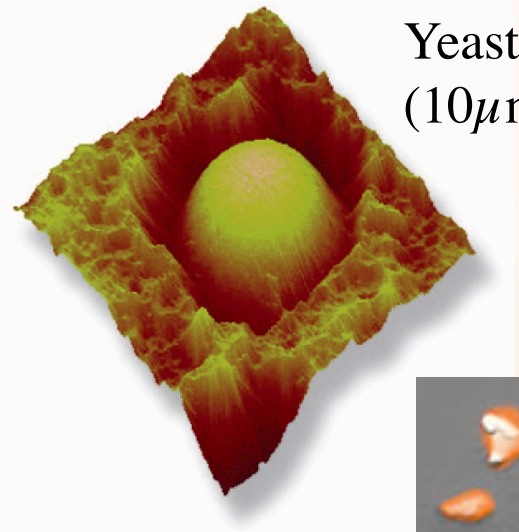

Yeast spore into a membrane
(10μm x 10μm)

Blood cells (tapping)

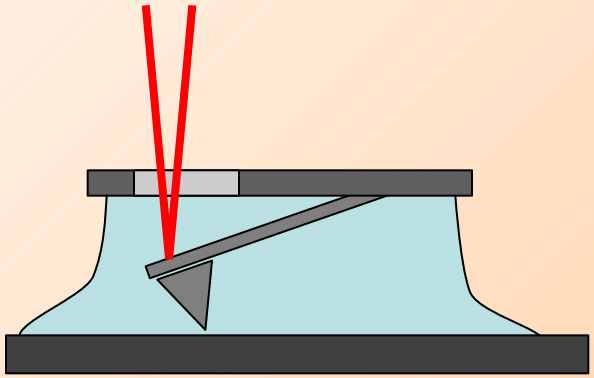

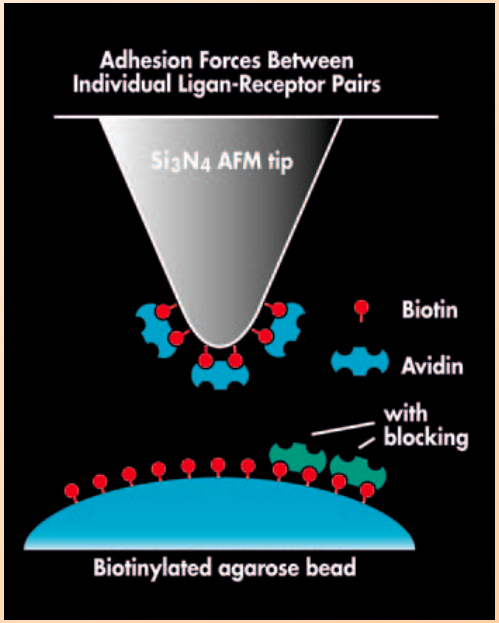

Force-Volume analysis

Identification and location of a protein on bacterial membrane

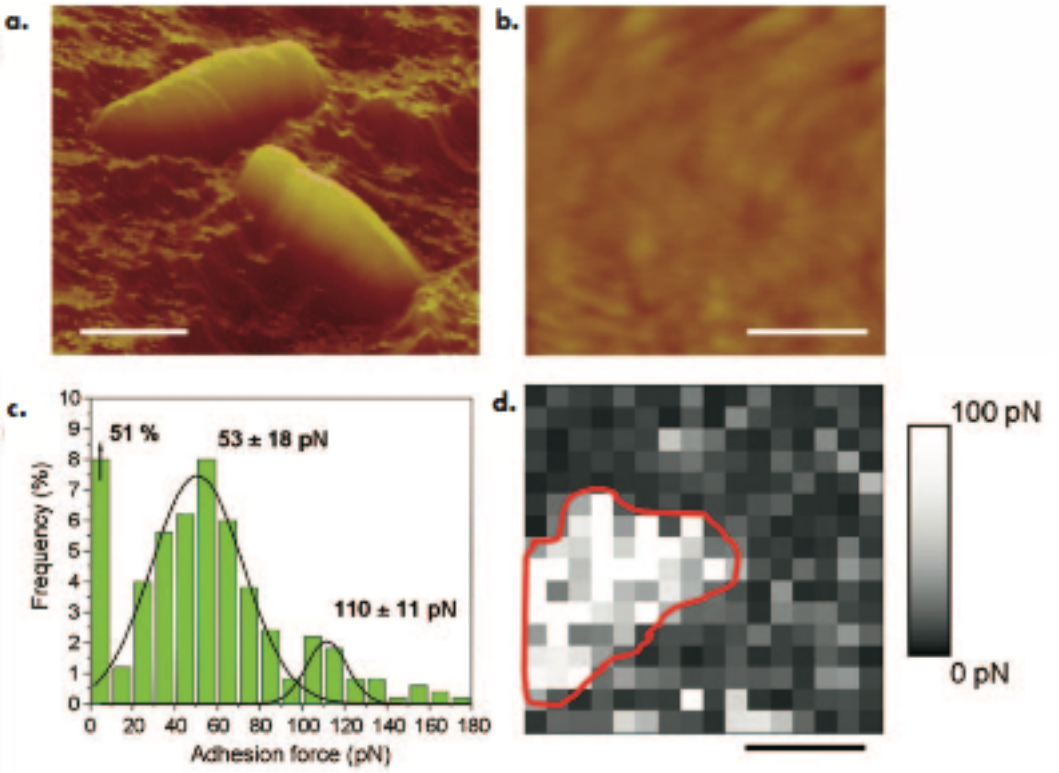

Figure 4. (a) AFM topographic image recorded in PBS showing two *M. bovis* BCG cells on a polymer substrate (scale bar: 2 μm). (b) Higher magnification image of the cell surface (scale bar: 100 nm). (c) Histogram and (d) spatially resolved map of adhesion forces recorded with a heparin tip (scale bar: 100 nm). Single HBHA adhesins were detected and found to be organized in nanodomains (red line). Adapted with permission from Nature Methods[3].

@ DOI 10.1002/sca.20177

Force-volume imaging

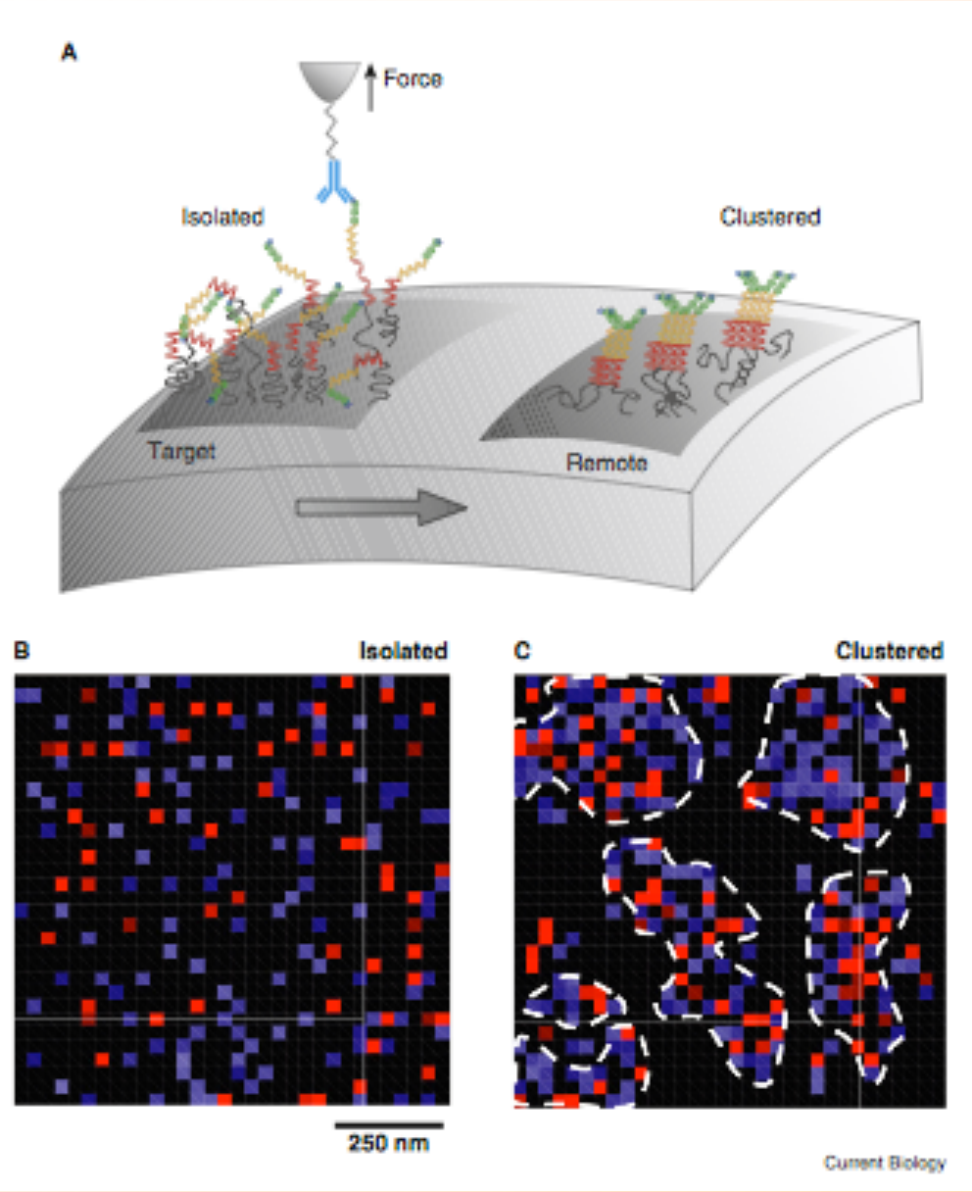

Figure 2. Imaging the dynamic clustering of cell-adhesion proteins on the surface of a living cell. (A) Single *C. albicans* adhesins were localized and stretched on different locations of a single yeast cell using an AFM tip bearing specific antibodies. (B) Molecular recognition map record- ed on a cell that was never probed, thus not subjected to force. Coloured pixels document the detection of single proteins (the blue and red pixels correspond to forces in the 0–150 pN and 150–300 pN range, respectively). Most proteins were isolated and evenly distributed, without any clear evidence for clustering. (C) Subsequent recognition map recorded on a remote area of the same cell following application of force. Proteins in the second map were no longer isolated but clustered into nanodomains referred to as 'nanoadhesomes'. Reprinted with permission from Alsteens, D. *et al.* (2010).

@Current Biology vol21 n6 R212, D.D Müller, Y.F. Dufrêne

Force-volume imaging

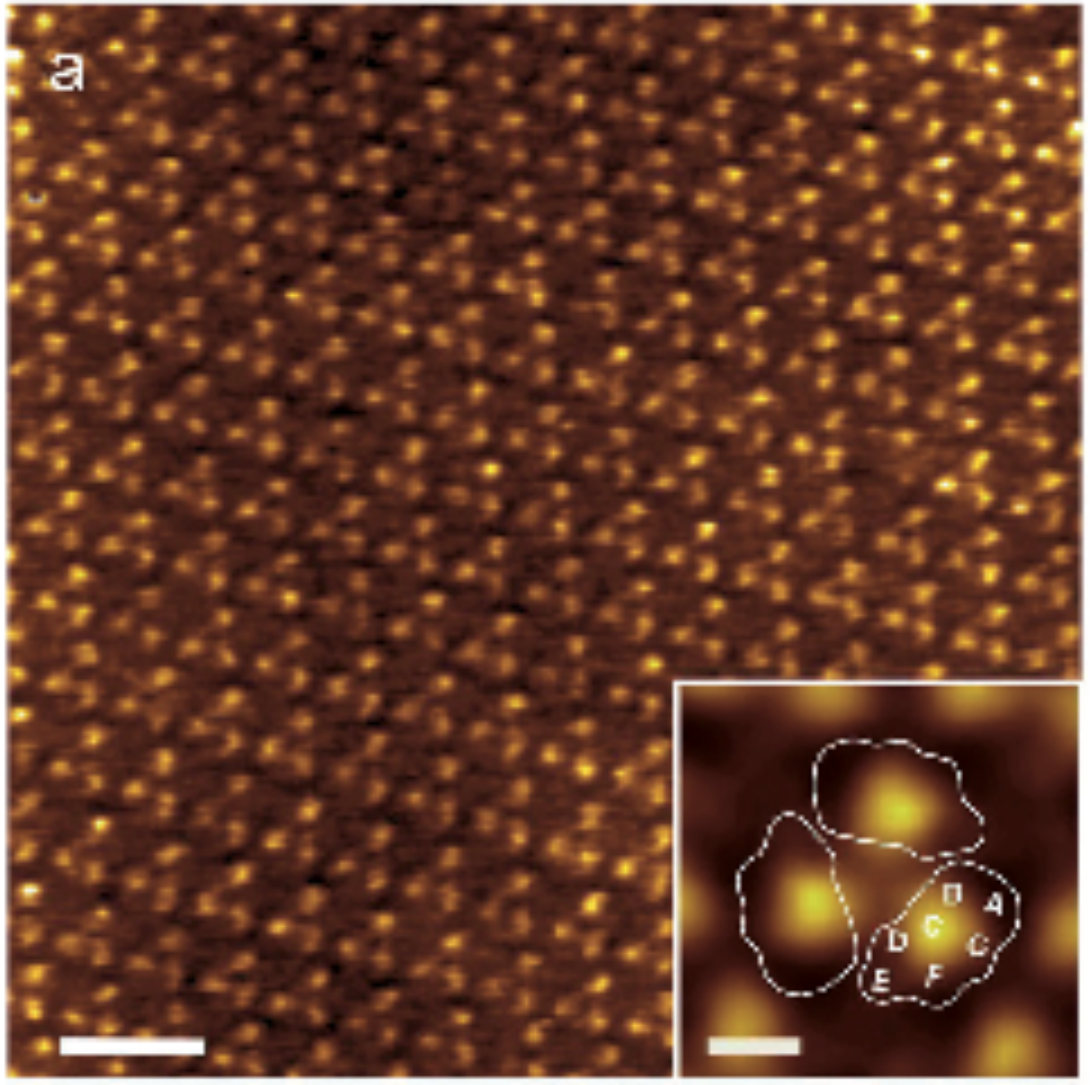

High-resolution force–volume AFM of the extracellular PM surface. a) Topography. Inset of (a) shows three-fold symmetrized cross-correlation average (n = 200) of the bacteriorhodopsin (BR) trimer. Outlined BR shapes (white lines with the seven transmembrane α-helices A–G indicated) were obtained from X-ray and electron crystallographic analyses.[15b] Full color scales correspond to vertical ranges of a) 1.0 nm. Scale bars, 10 nm (raw data) and 2 nm (insets).

@ DOI: 10.1002/anie.201103991

Tapping mode in fluid

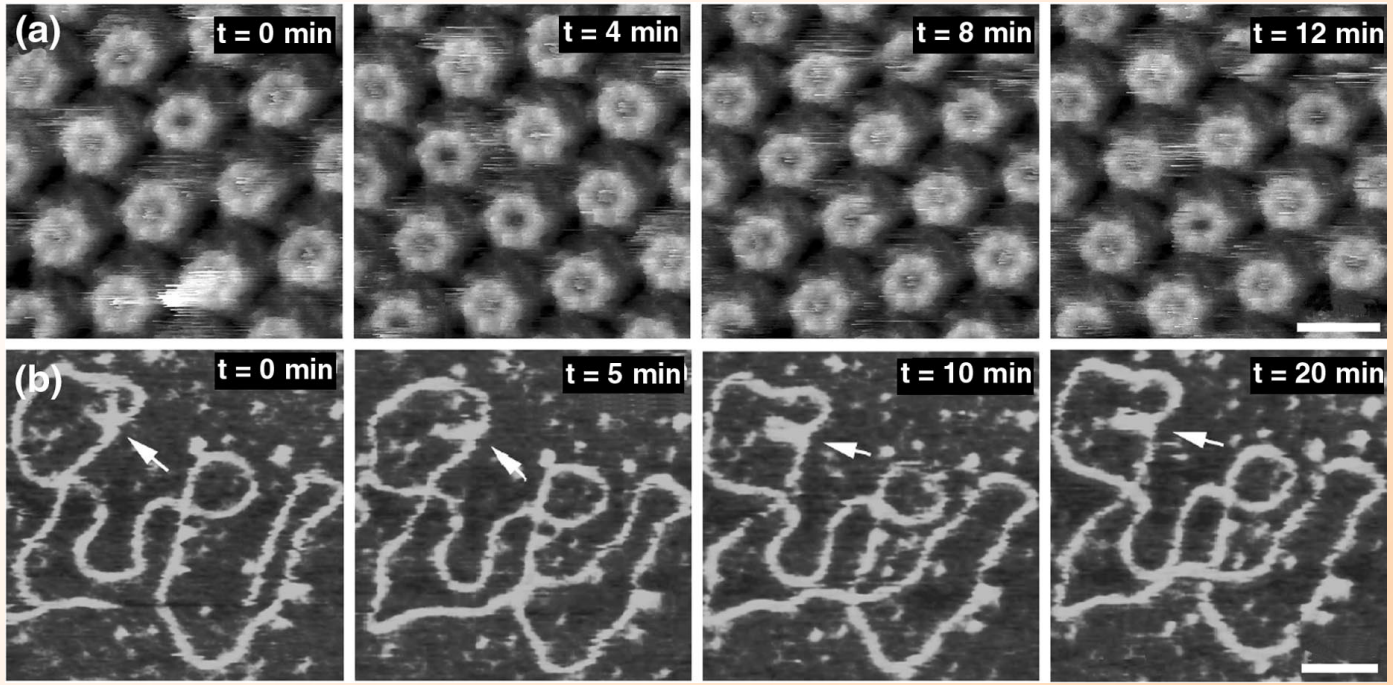

Conformational changes of proteins (streptavidin) and DNA observed in buffer solution. (a) The hexagonally packed intermediate (HPI) layer consists of hexameric units having a central core and connecting arms. At the inner surface, the cores exhibit a central pore that occurs in 'open' (unplugged) and 'closed' (plugged) conformations. Repeated imaging of the same surface at 4-min intervals showed that some pores changed their conformation. This conformational change was fully reversible and could be observed over long time periods. The defective pore at the bottom left corner is used as a reference to align the scans. The images were recorded in 100 mM KCl, 20 mM MgCl2, 10 mM Tris, pH 8.2, using the contact mode. Bar, 15 nm. Shades correpond to a height range of 6 nm. (b) Atomic force microscope images of plasmid DNA. This plasmid contains a 106-bp inverted repeat, which is stabilized in the cruciform conformation by negative DNA supercoiling. Arrows indicate the cruciforms. The frames from the left to right are four repetitive scans over the same area. The hairpin arms of the indicated cruciform were initially quite far away from each other (with an angle of ~100**8), but then they** moved closer and finally adopted a parallel orientation. The scanning was performed in Tris–EDTA buffer with a NanoScope III MultiMode system (Digital Instruments, Inc., Santa Barbara, CA, USA) operating in the tapping mode. Bar, 40 nm.

@trends in CELL BIOLOGY (Vol. 9) February 1999

Fluorescence imaging and AFM

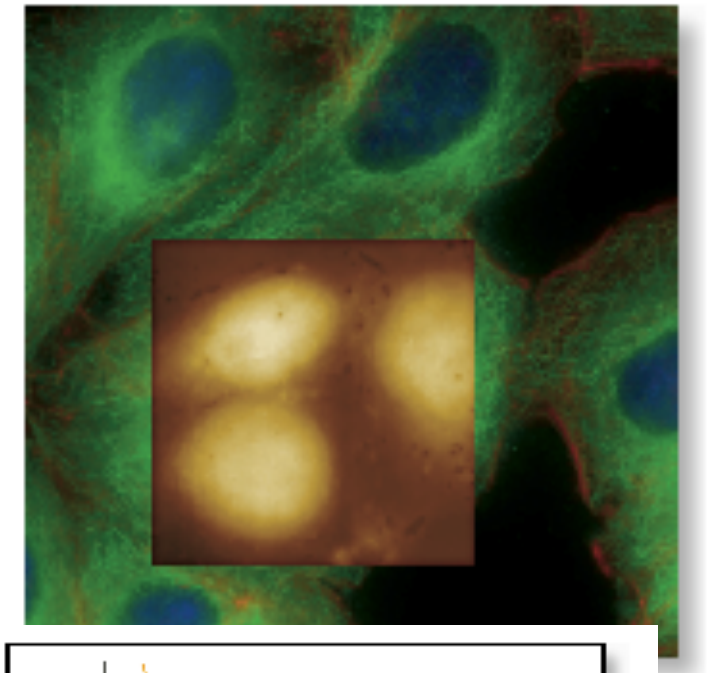

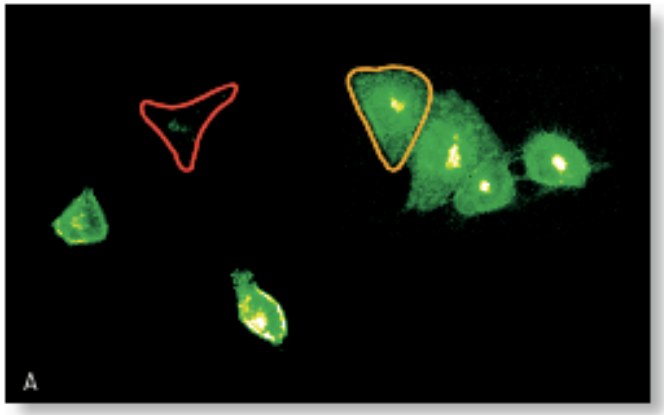

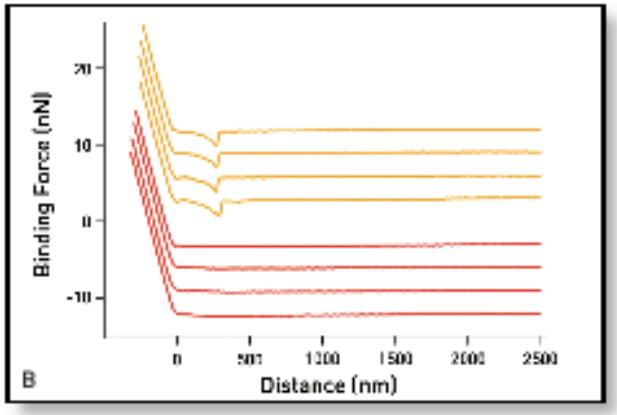

HeLa cells were transfected to express a fluorescent membrane protein. (A) Fluorescence intensity varied from strong (yellow circled cell) to faint (red circled cell), corresponding to varying degrees of protein expression. (B) Force measurements performed with functionalized AFM probes showed a strong correlation between binding force and fluorescence intensity, with bright cells yielding many binding events (yellow curves) and dimmer cells yielding very few (red curves). Data courtesy of Frank Lafont and Joëlle Warein, Institut Pasteur de Lille, France.

Nanolithography and nanomanipulation

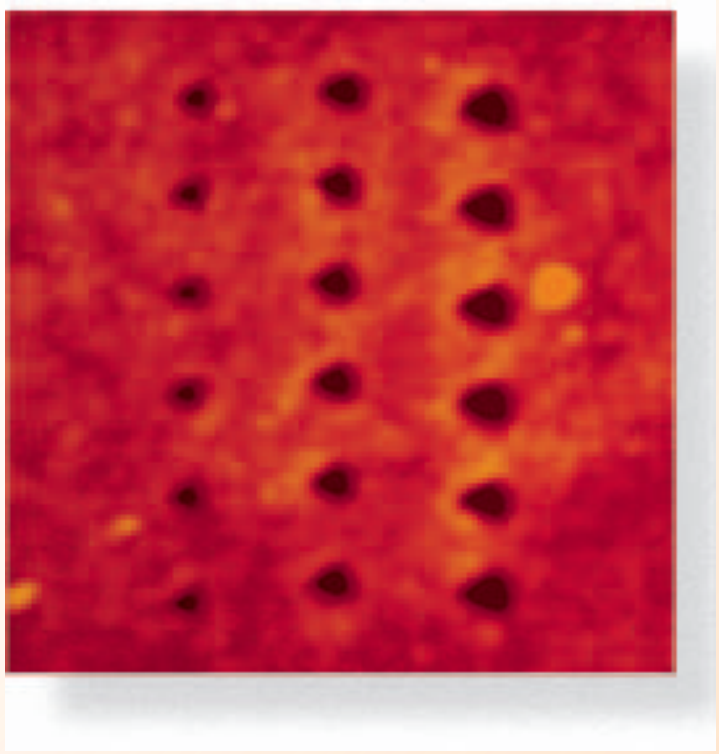

Nanoindentation (15 nm)
in polymer film
(800nm x 800 nm)

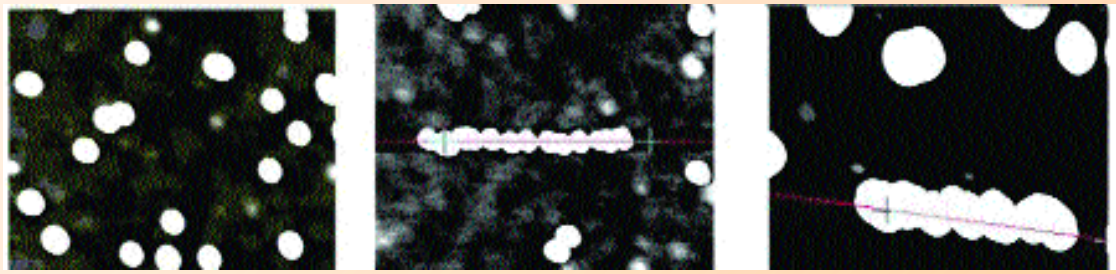

Gold nanoparticles manipulation (8nm)

Nanomechanical imaging

Tapping phase imaging of copolymer

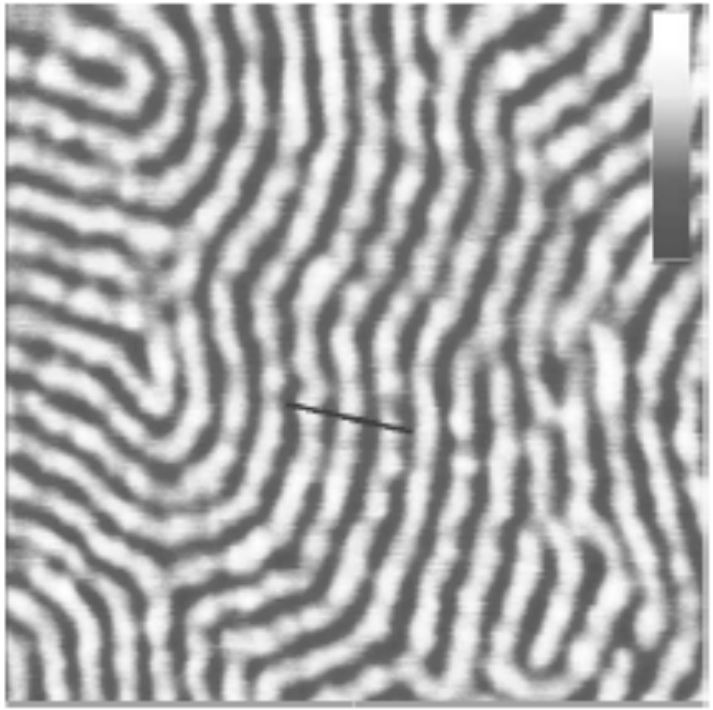

Fig. 10. Phase image of the copolymer (500 nm × 500 nm). The contrast bar (upper right) corresponds to 5 degrees. The fits are carried out on curves recorded on different locations along the black line.

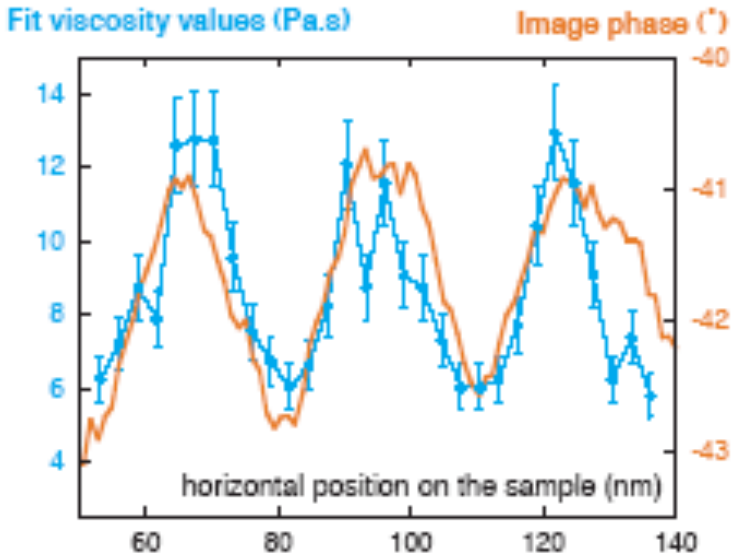

Fig. 11. Comparison of the phase image section and the viscosity values obtained from the fits. The fits values (with 10% relative error) follow the same variations as the image phase contrast, thus reproducing the local variations of the mechanical properties. The lateral resolution is close to the step between two adjacent measurements, *i.e.* about 3 nm.

@https://doi.org/10.1021/la0005098

PeakForce Tapping

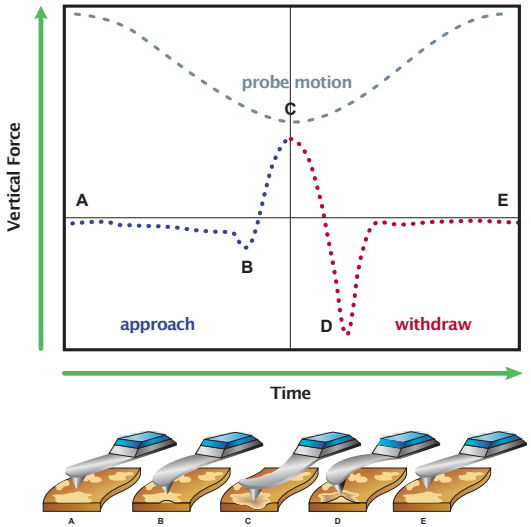

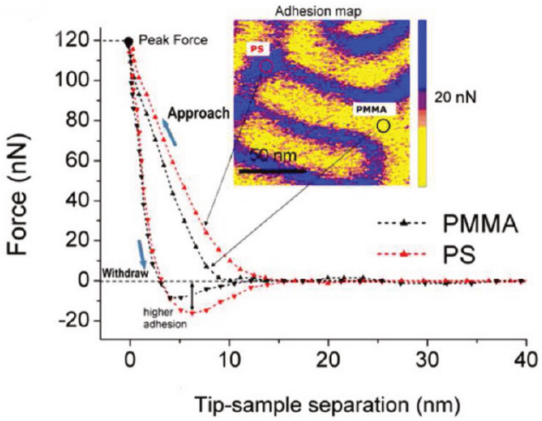

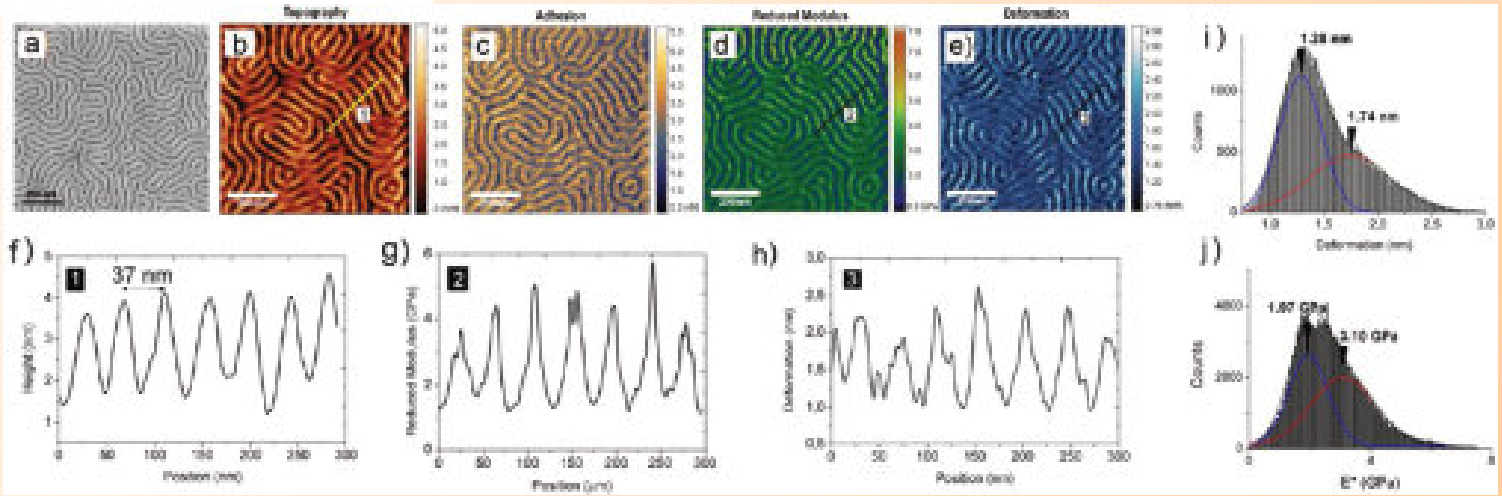

Figure 5. Characterization of a self-assembled L37PS-b-PMMA BCP thin film sample: (a) SEM image of the film after the PMMA phase has been removed by oxygen plasma and then height (b), adhesion (c), elastic (d), and deformation (e) maps of the same sample acquired by peak force tapping at a 30 nN set point. In the graphs below we report the detailed profiles of the topography (f), reduced modulus (g), and deformation (h), with the profiles indicated as 1, 2, and 3, respectively. For deformation and elastic maps the corresponding Gaussian fittings of the data histograms are also reported in (i) and (j). *@https://doi.org/10.1021/acs.langmuir.5b02595*

EFM (Electric Force Microscope)

Applications in nanoelectronics

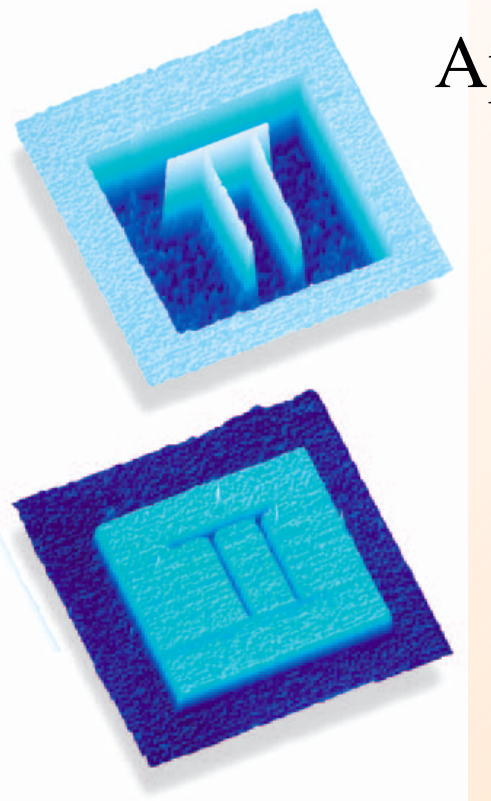

EFM images for 2 inverted polarisation

(15μm x 15 μm)

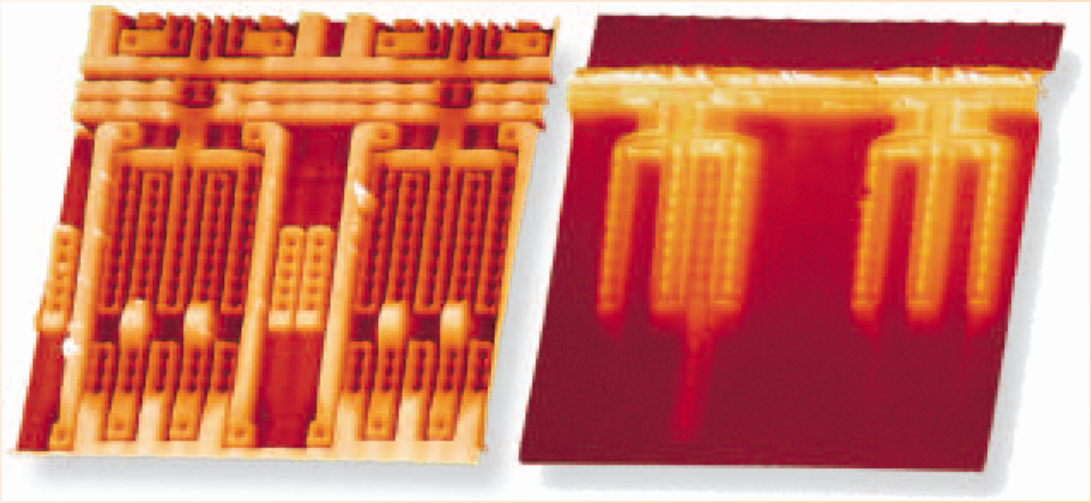

Transistor default detected by EFM
(80μm x 80 μm)

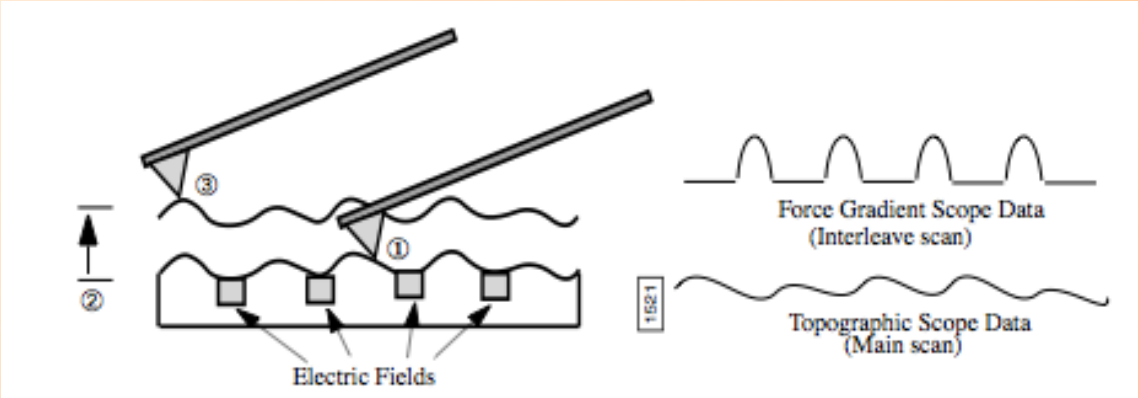

MFM (Magnetic Force Microscope)

Double pass imaging

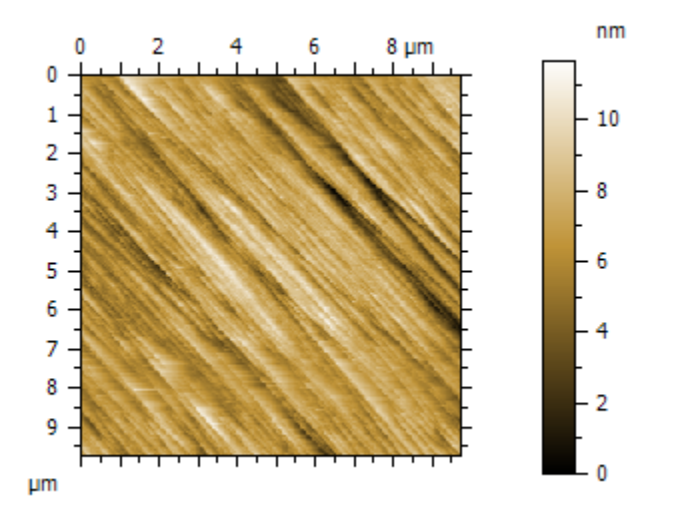

topography

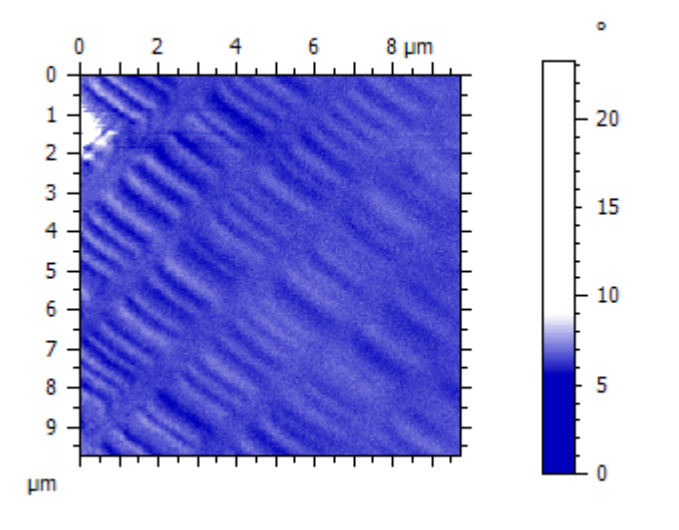

MFM image

Hard disk surface

SThM (Scanning Thermal Microscope)

AFM thermal probe

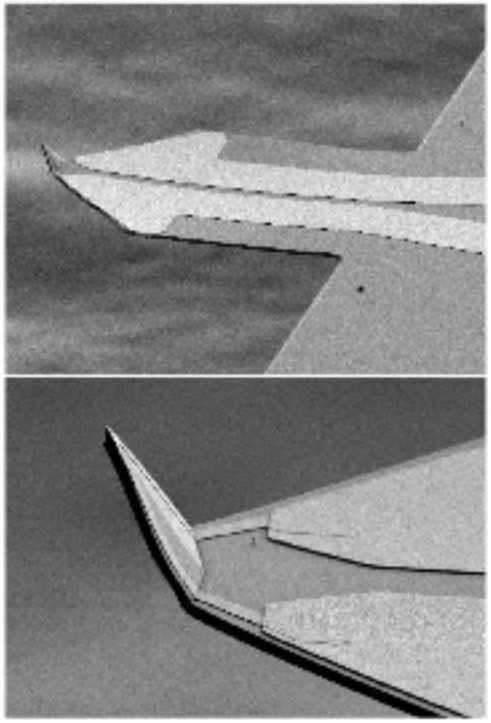

SEM Images of the entire cantilever (top) and the tip (bottom)

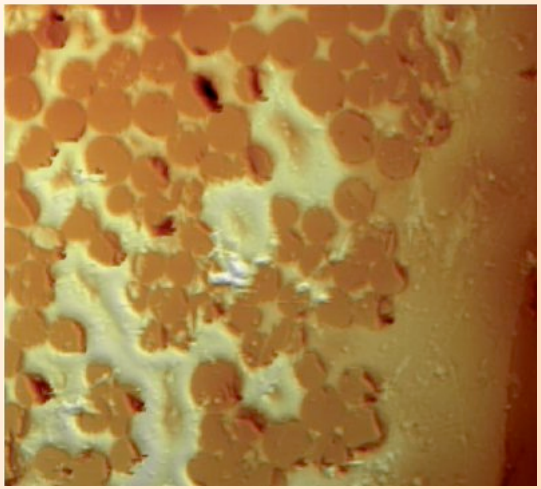

topography

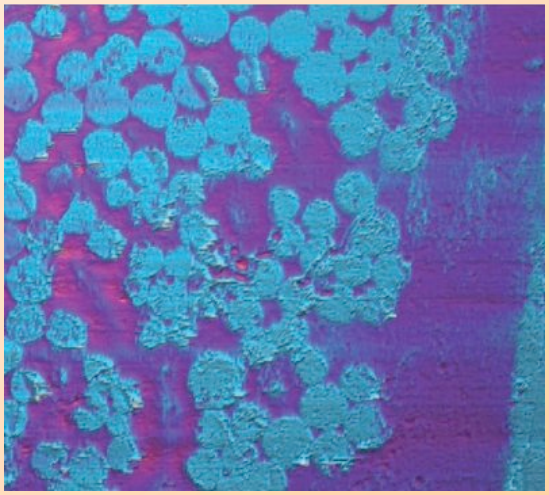

Thermal conductivity image

Sample of glass fibers into epoxy matrix.

Coupling AFM/STM in high vacuum

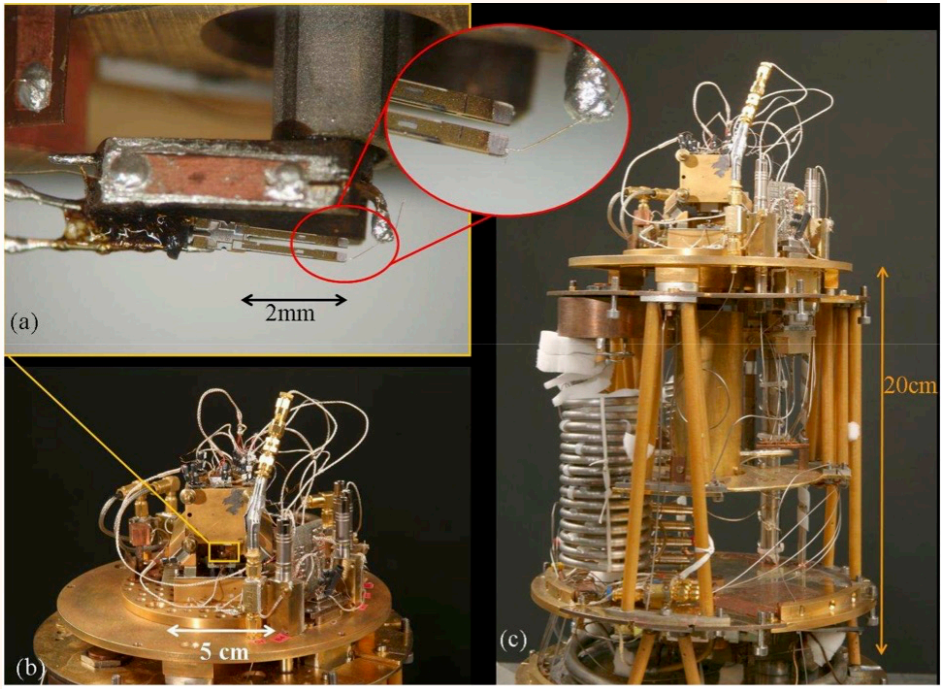

@H. Le Sueur. Cryogenic AFM-STM for mesoscopic physics. Condensed Matter. Université Pierre et Marie Curie - Paris VI, 2007.

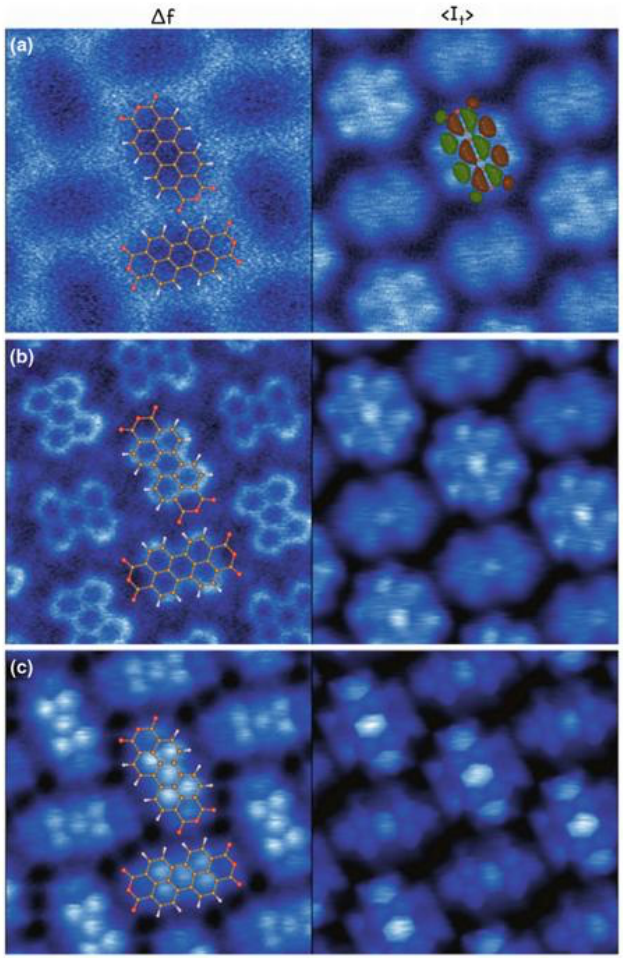

Fig. 3.1 Simultaneous AFM/STM images obtained with Xe-functionalized probe of herringbone monolayer of PTCDA molecules deposited on Ag(111) surface acquired with Kolibri sensor at 1.2 K in different tip-sample distances. Figures show the evolution of the frequency shift (*left*) and average tunneling current (*right*) while decreasing the tip-sample distance. Skeleton of PTCDA molecule is superimposed over AFM images to facilitate recognition of the high-resolution contrast. In the *right top figure*, real-space distribution of the LUMO orbital obtained from DFT calculations is shown in order to underline its good agreement with the STM contrast at this distance

AFM-IR : coupling AFM with IR spectroscopy

IR laser

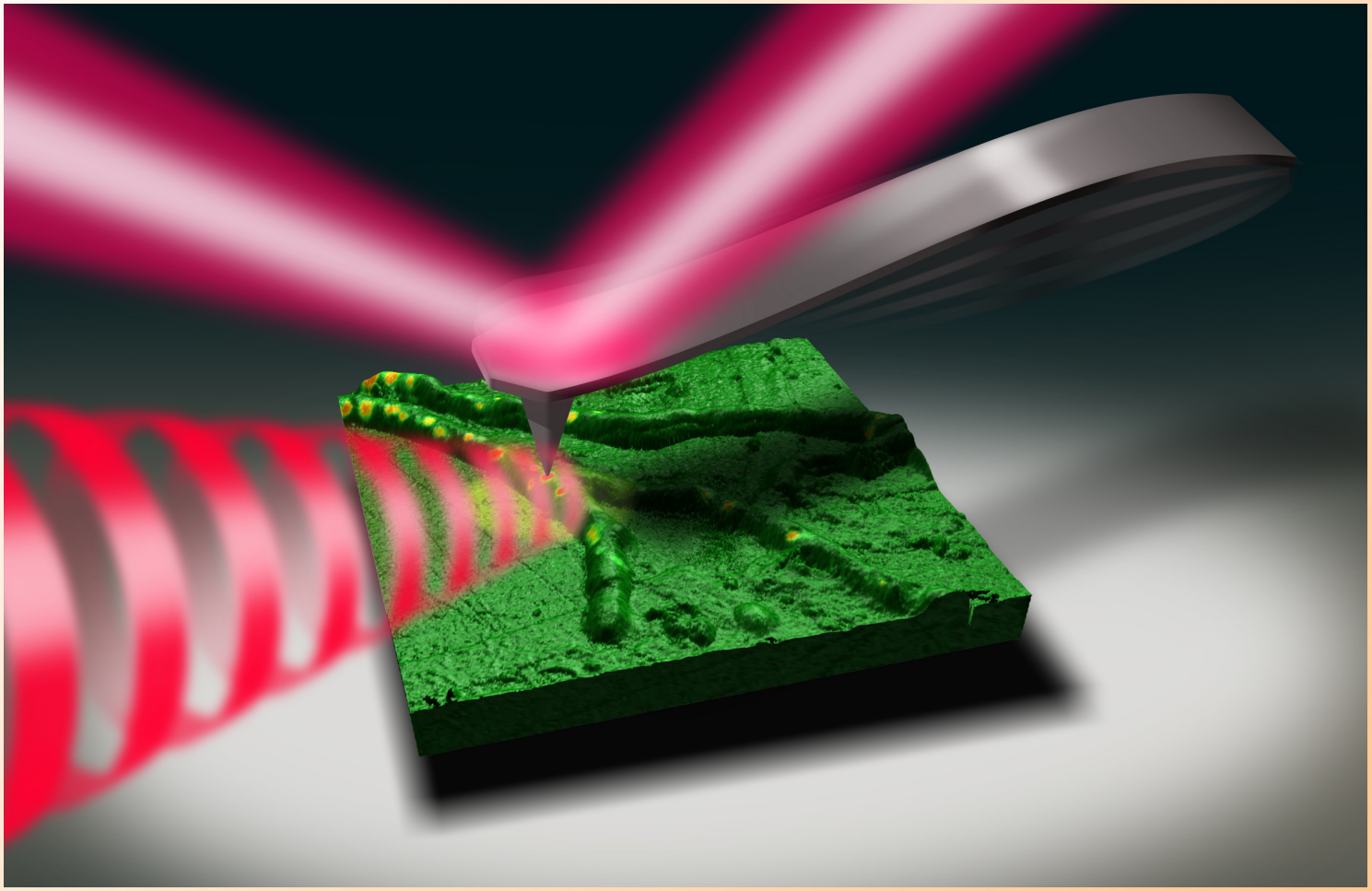

Field of applications - Biology

TISSUE – Human cells

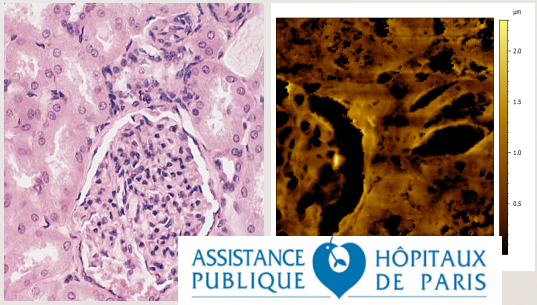

ASSISTANCE PUBLIQUE HÔPITAUX DE PARIS

Calcification in human tissues

Extracellular vesicles

Penetration of nanocarriers

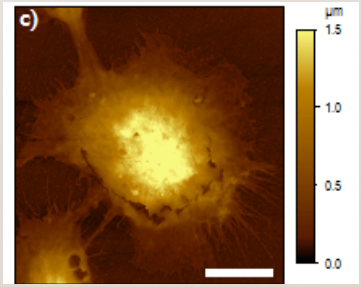

Nanoparticules and cell: macrophage

L'ORÉAL

Fine structure of the hair…

MICRO-ORGANISMS

Accumulation of biopolymer or lipids

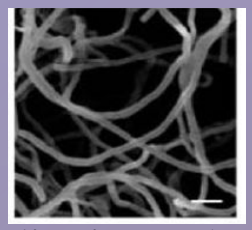

I2BC

Localisation and quantification

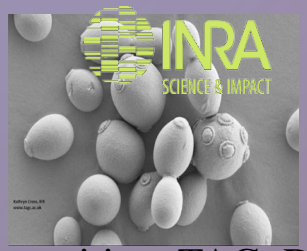

Local composition, TAG, DAG, MAG and FFA differentiation

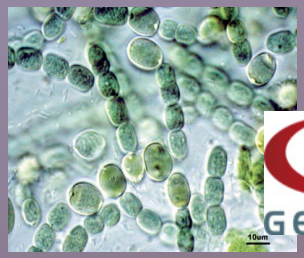

NANOMETRIC SCALE

Protein assemblies

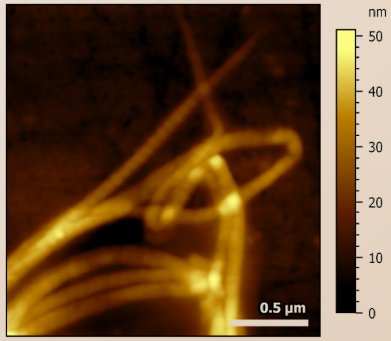

Collagen fibrils denaturation

System complex: Collagen-antibiotic

UPMC SORBONNE UNIVERSITÉS

Bacterial amyloids

Beta structure of amyloids

Prion, lipids bilayer

ULB UNIVERSITÉ LIBRE DE BRUXELLES

INRA SCIENCES & IMPACT

Field of applications

Polymers sciences

Multilayers: Structure-cristallinity

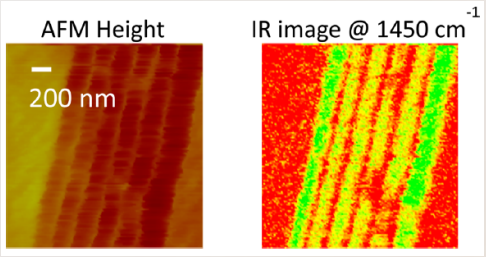

A Dazzi, Chem Rev, 2016

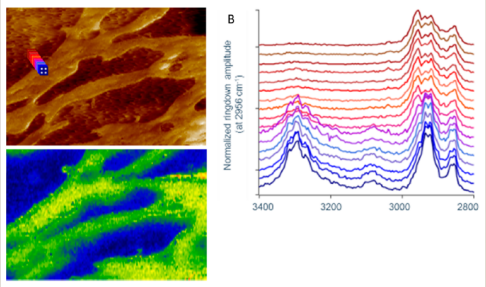

Trace of adjuvant blooming

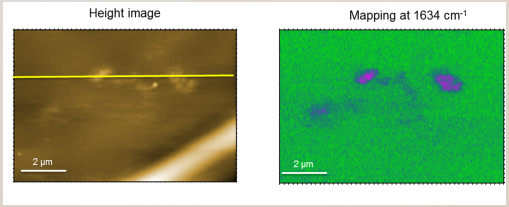

A Dazzi, International journal of pharmaceutics Volume 484, Issues 1–2, 2015

Heritage sciences

- Investigate parchments degradation

G.Latour, Scientific Report, 2016

- IR signatures: heterogeneities in ancient tissues or violin sections

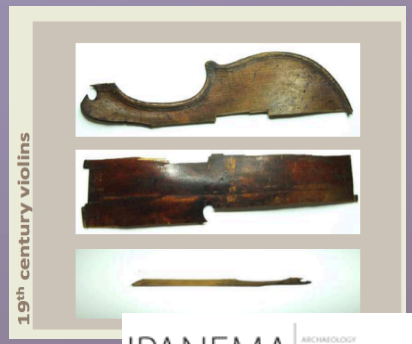

IPANEMA ANCIENT MATERIALS RESEARCH PLATFORM

Nanoparticles

- Polymeric Nps

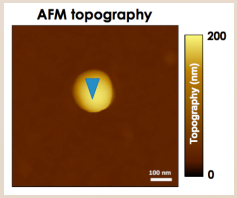

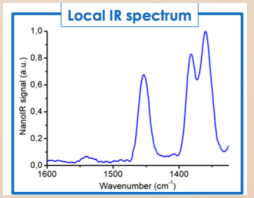

Mathurin J., 10.1039/C8AN01239C, Analyst, 2018

Astrochemistry

- Investigation of organic matter in micrometeorites

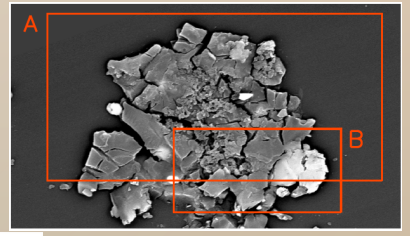

J. Mathurin, A&A, 2019